STABILITY OF THE NON-ISOTHERMAL TAYLOR-COUETTE FLOW OF A FERROFLUID UNDER EXTERNAL MAGNETIC FIELD

by

Yavuz Emre Kamış

B.S., Mechanical Engineering, Boğaziçi University, 2014

Submitted to the Institute for Graduate Studies in
Science and Engineering in partial fulfillment of
the requirements for the degree of
Master of Science

Graduate Program in Mechanical Engineering
Boğaziçi University
2018

ABSTRACT

STABILITY OF THE NON-ISOTHERMAL TAYLOR-COUETTE FLOW OF A FERROFLUID UNDER EXTERNAL MAGNETIC FIELD

A stability analysis is conducted for the non-isothermal Taylor-Couette flow of a non-conductive ferrofluid under the action of an azimuthal magnetic field. The transition from steady flow to Taylor vortex flow is investigated in terms of the critical Taylor number and with respect to the changes in the magnetic field strength, radial temperature gradient, gap ratio, ferroparticle concentration and size. For the linear stability analysis, infinitesimal perturbations to the velocity, temperature and magnetization fields are considered and the resulting linear system of stability equations is solved using Chebyshev collocation method. Also, the original nonlinear system of equations is solved numerically using a finite element analysis software, and the results are compared with the linear stability analysis results. A significant stabilization is observed under strong magnetic fields for all cases. It is also observed that radial temperature difference has a destabilizing effect on the flow and this effect is amplified when the magnetic field strength is increased. Higher ferroparticle volume fraction and size lead to a strong degree of magnetization of the fluid and amplifies the stabilizing effect of magnetic fields. The stabilization under azimuthal magnetic forces is observed to be smaller for the narrow gap case compared to the wide gap case.

ÖZET

HARİCİ MANYETİK ALAN ALTINDAKİ FERRO-AKIŞKANIN İZOTERMAL OLMAYAN TAYLOR-COUETTE AKIŞININ KARARLILIĞI

Azimutal manyetik alan hareketi altındaki iletken olmayan ferro-akışkanın izotermal olmayan Taylor-Couette akışı üzerine bir kararlılık analizi yürütülmüştür. Sabit akıştan Taylor spiral akışına doğru olan geçiş, kritik Taylor sayısına göre manyetik alan kuvveti, dairesel sıcaklık eğimi, boşluk oranı, ferro-parçacık derişimi ve boyutu açısından incelenmiştir. Doğrusal kararlılık analizi için; hız, sıcaklık ve manyetizasyon alanlar üzerindeki ölçülemeyecek derecede küçük sarsımlar göz önünde bulundurulmuş ve bunun sonucunda çıkan doğrusal kararlılık denklemleri sistemi Chebyshev kollokasyon metodu kullanılarak çözülmüştür. Ayrıca, orijinal doğrusal olmayan denklemler sistemi, sonlu eleman analiz yazılımı ile sayısal olarak çözülmüştür ve sonuçlar doğrusal kararlılık analizi sonuçları ile karşılaştırılmıştır. Güçlü manyetik alan altındaki tüm durumlarda anlamlı bir kararlılık gözlemlenmiştir. Ayrıca, dairesel sıcaklık farkının akış üzerinde kararlılığı bozan bir etkisi olduğu ve bu etkinin manyetik alanın gücü arttırıldıkça yükseldiği gözlemlenmiştir. Yüksek ferro-parçacık derişimi ve boyutu, akışkanın güçlü derecede manyetize olmasına sebep olmaktadır ve manyetik alanların kararlılaştırıcı etkisini yükseltmektedir. Geniş boşluklu durumla karşılaştırıldığında, azimutal manyetik kuvvet altındaki kararlılığın dar boşluk durumu için daha düşük olduğu gözlemlenmiştir.

TABLE OF CONTENTS

LIST OF FIGURES

LIST OF TABLES

LIST OF SYMBOLS

$\mathbf{B}$	Magnetic flux density vector
c	Specific heat capacity
c_M	Langevin magnetic scale parameter
d	Ferroparticle diameter
D	Differentiation matrix
D_B	Brownian diffusivity
$\mathbf{E}$	Electric field
F	Helmholtz free energy per unit volume
F'	Helmholtz free energy per unit mass
$\mathbf{H}$	Magnetic field vector
H_c	Coercive field
$\mathbf{H}_0$	External magnetic field vector
I	Electric current
J	Volume density of moment inertia
$\mathbf{J}_e$	External current denity vector
$\mathbf{J}_i$	Induced current density vector
k	Wave number
k_f	Thermal conductivity of the base fluid
$\mathbf{m}$	Magnetic dipoles
$\mathbf{M}$	Magnetization vector
M_d	Bulk magnetization
M_{eq}	Equilibrium magnetization
M_r	Remanent magnetization
p	Pressure
Pr	Prandtl number
Q	Heat content

R_M	Ferrohydrodynamic number
R_H	Relaxation number
Re	Reynolds number
$\mathbf{S}$	Surface normal vector, Internal angular momentum vector
S'	Entropy change per unit mass
Sc	Schmidt number
T	Temperature field
$\mathcal{T}'_m$	Magnetic fluid stress tensor
Ta	Taylor number
$\mathbf{u}$	Velocity vector
U'	Internal energy per unit mass
v	Specific volume
α_L	Langevin parameter
ζ	Gap ratio
η	Dynamic viscosity
η'	Spin viscosity
μ_0	Magnetic permeability of free space
μ_r	Relative magnetic permeability
ρ	Density of the ferrofluid
ρ_f	Density of the base fluid
ρ_p	Density of the ferroparticle
σ	Amplification factor
σ_c	Electrical conductivity of the medium
τ_B	Brownian relaxation time
τ_S	Spin relaxation time
ϕ	Volume fraction of the ferroparticles
χ	Magnetic susceptibility

LIST OF ACRONYMS/ABBREVIATIONS

2-D	Two Dimensional
CF	Couette flow
ODE	Ordinary Differential Equation
PVD	Physical Vapor Decomposition
TVF	Taylor vortex flow

1. INTRODUCTION

1.1. Ferrofluids

Nanofluids have been studied extensively over the years for enhanced heat transfer effects. The modification of the thermo-physical properties by the colloidal suspension of particles in a base fluid, allows its use and application in energy supply, photonics and transportation. Nanofluids show better stability aspects when compared to suspensions made by micrometer or millimeter sized particles because of size effect and Brownian motion [1]. Typically, a nanofluid suspension will consist of a base-fluid(water, ethylene glycol or oil) and nano-sized particles which can be metallic (Cu, Al, Fe, Au and Ag) or non-metallic compounds (Al_2O_3, CuO, Fe_3O_4, TiO_2 and SiC) whose thermal properties are summarized in Table 1.1. Nanofluid preparation is also an active topic of research.

Table 1.1. Thermal Properties of Selected Materials for nanofluid preparation [1]

Material		Thermal Conductivity(W/m*K)
Metallic Solids	Cu	401
	Al	237
	Ag	428
	Au	318
	Fe	83.5
Nonmetallic Solids	Al_2O_3	40
	CuO	76.5
	Si	148
	SiC	270
Base Fluids	H_2O	0.613
	Ethylene Glycol	0.253
	Engine Oil	0.145

Basically the two physical challenges during this process is obtaining the nanosized particles and synthesizing a stable suspension of the nanoparticle inside the base fluid. There two main method of preparing nanofluids reported in the literature.

The single-step method aims to combine these two processes, the nanoparticles are directly prepared by physical vapor deposition (PVD). With this method, the intermediate steps of preparing the nanoparticle which are drying, storage, transportation and dispersion are avoided, so the agglomeration is minimized, but it is applicable for only low vapor pressure (non-volatile) base fluids [1]. This technique was introduced by Akoh *et al.* in [2] and successfully applied by Eastman *et al.* in [3] by condensating Cu nanoparticles in ethylene glycol.

The two-step method consists of dispersing the available nanosized particles into base liquids. The nanoparticles are first produced as dry powder and then dispersed into the fluid as a second step. An advantage of this method is that the manufacturing techniques for dry nanosized powder are well understood and established in industrial level. However, the suspension obtained after dispersing the nanoparticle is subject to agglomeration and instability. To improve stability, addition of surfactants and ultrasonic agitation are among the most selected techniques. Xie *et al.* [4] have prepared nanofluids with the two step method using alumina particles and water, ethylene gylcol and oil as base fluid. Magnetic force agitation and ultrasonification were used to increase stability.

Ferrofluids are colloidal suspensions of nano-sized ferroparticles(e.g.magnetite Fe_3O_4 particles) in a carrier liquid. These fluids, having strong susceptibility to external magnetic field, are used in many applications in heat and flow control. A common usage is in the high-power loudspeakers where the ferrofluid can effectively remove heat from the speaker coils and improve the sound quality by damping the resonances. [6, 7] Ferrofluids can also be used in damping applications in civil engineering where damping

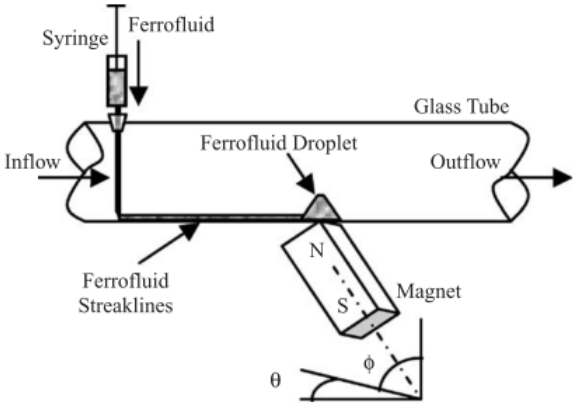

Figure 1.1. Experimental setup of Ganguly *et al.* [5]

of seismic activity is essential or in automotive industry where damping of rough road conditions is important. [7] Recent studies suggest the magnetic forces can be used as a body force to control flow fields, [8] where non-contact mixing can be achieved, as in boundary layer control for high Reynolds number flow. [9] Ferrofluids are also popular in biomedical applications, especially in magnetic drug targeting [10], that is, applying magnetic field to alter the flow field of blood containing drugs coated with ferromagnetic particles. Nacev *et al.* [11] investigated the ferromagnetic particle flux numerically in and around the blood vessels, solving the mass transfer problem taking into account magnetic slip mechanisms. Ganguly *et al.* [5] have conducted a similar study, solving for ferrofluid flow and mass transfer problem under applied magnetic field for drug targeting applications and verifying it with experiments whose setup is shown in Figure 1.1. Li *et al.* [12] also contributed to the subject, investigating a 2-D rectangular channel flow under the magnetic field of a circular cross-section magnet with vertical magnetization.

A common research interest in the literature is to find out how a body force affects boundary layer, in our case that would be magnetic or electric forces. Takhar *et al.* [13] studies an unsteady, laminar boundary layer of a stagnation flow with magnetic field normal to the surface. The partial differential equations(continuity, momentum and energy equations) are transformed to ordinary differentials using similarity variables

and the system is solved by shooting technique, which is very common in boundary layer analysis. Andersson *et al.* [14] also conducted a steady BL analysis over a stretching sheet with the magnetic field of a point dipole with prescribed temperature boundary condition whose geometry is shown in Figure 1.2. They include magnetocaloric and viscous disspation effects in the energy equation. One of the more recent analyses by Ghasemi *et al.* [15] studies the steady non-isothermal boundary layer flow over a stretching cylinder with the magnetic field radially outwards. The obtained ODE system is solved by Differential Quadrature method. Another study by Dash *et al.* [16] covering a stagnation flow onto a stretching sheet includes particle diffusion effects with chemical reaction source term.

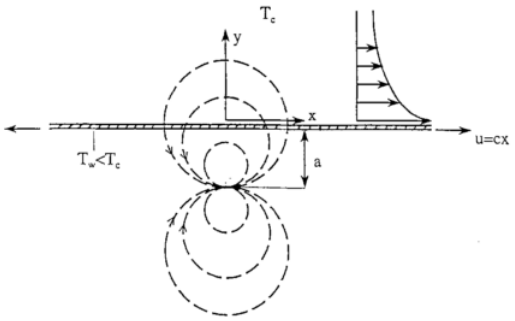

Figure 1.2. The geometry of the problem in [14]

1.2. Theoretical Background on Ferrohydrodynamics

1.2.1. Magnetization and Magnetic Materials

Magnetization results from microscopic currents that arises from atomic motions. Just like small charge displacement inside a material gives rise to a polarization field, these small currents will give rise to magnetization. A general relation for the total magnetization vector of a body can be obtained by summing the magnetic dipoles, $\mathbf{m}$, as

$$\mathbf{M} = N\mathbf{m} = NId\mathbf{A}\left[\frac{A}{m}\right] \tag{1.1}$$

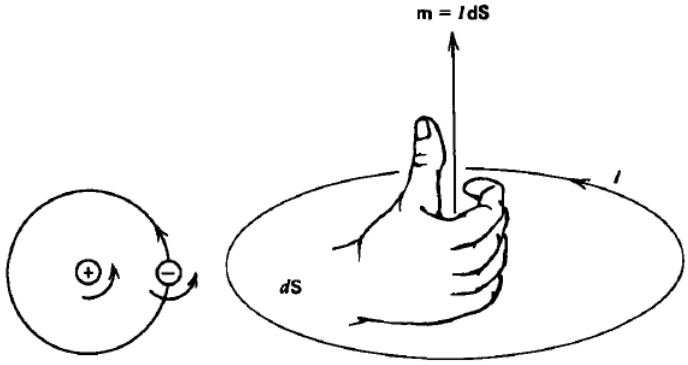

Figure 1.3. Schematic of the atomic currents and its resultant magnetization which constitutes a magnetic dipole [17]

where N is the number density of the circulating current loops.

To obtain expressions for the magnetization vector $\mathbf{M}$ of the magnetic materials, Lorentz force is applied to the applied field $\mathbf{H}$ and the atomic currents [17].

It is physical to assume linearity between magnetization and the applied magnetic field in steady state, $\mathbf{M} = \chi\mathbf{H}$ where χ is the magnetic susceptibility. When substituted in the constitutive relation $\mathbf{B} = \mu_\mathbf{0}(\mathbf{M} + \mathbf{H})$ we obtain

$$\begin{aligned} \mathbf{B} &= \mu_0(\chi\mathbf{H} + \mathbf{H}) \\ &= \mu_0(1+\chi)\mathbf{H} \\ &= \mu_0\mu_r\mathbf{H} \end{aligned} \tag{1.2}$$

where $\mu_r = 1 + \chi$ is the relative permeability of the material. In free space, $\chi = 0$ and $\mu_r = 1$. It can also be a function of the magnetic field and temperature, depending on the magnetic equation of state of the domain.

1.2.1.1. Diamagnetism. Diamagnetic effects are usually very small but they exist in all materials because the dipoles with moments parallel to the applied field will undergo an increase in the orbit speed whereas the orbiting electron speed of the dipoles with

opposite moments will decrease.

Diamagnetism is basically the alignment of the magnetic moments in the opposite direction of the applied magnetic field. Hence, $-1 \ll \chi < 0$ is the range for diamagnetic susceptibility which shows diamagnetic effects are usually very small.

1.2.1.2. Paramagnetism. Paramagnetism is the alignment of the dipoles in the direction of the applied field. All the moments that are arbitrarily placed will feel a torque due to the angle between them and the applied field. Opposing to this torque is the thermal agitation of the particles. The competition of these two effects are described by the so-called Langevin relation

$$M = M_d(\coth(\alpha_L) - \alpha_L^{-1}) \tag{1.3}$$

$$= M_d L(\alpha_L) \tag{1.4}$$

where M_d is the equilibrium magnetization of the material and $\alpha_L = \frac{\pi}{6}\frac{\mu_0 M_d H d^3}{k_B T}$ is the Langevin parameter. Figure1.4 shows M-H curve for a paramagnetic material. In the limit $\alpha_L \ll 1$, Taylor series expansion shows $L(\alpha_L) = \alpha_L/3 = \chi$. In the asymptotic form where $\alpha_L \gg 1$ the Langevin function becomes

$$L(\alpha_L) = \left(1 - \frac{6}{\pi}\frac{k_B T}{\mu_0 M_d H d^3}\right) = \chi \tag{1.5}$$

1.2.1.3. Ferromagnetism. Ferromagnetic particles show very high coupling between the alignment of the dipoles and the applied magnetic field. This results in a nonlinear behaviour of the B-H curve which often exhibits hysteresis. As shown in Figure 1.5, ferromagnetic materials retain a remanent magetiation in the absence of field M_r and need a coercive field $-H_c$ to bring to zero magnetization [17].

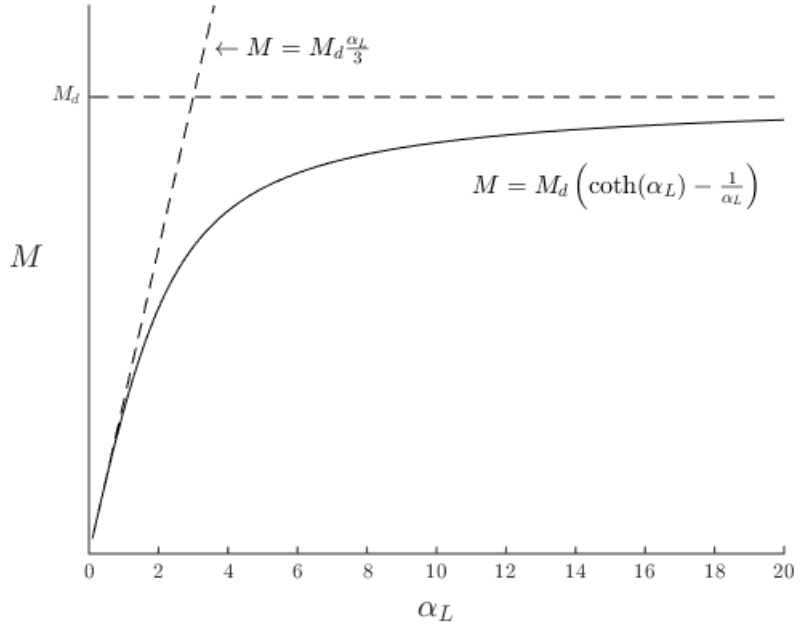

Figure 1.4. Variation of the magnetization of a paramagnetic material in accordance to the Langevin relation.

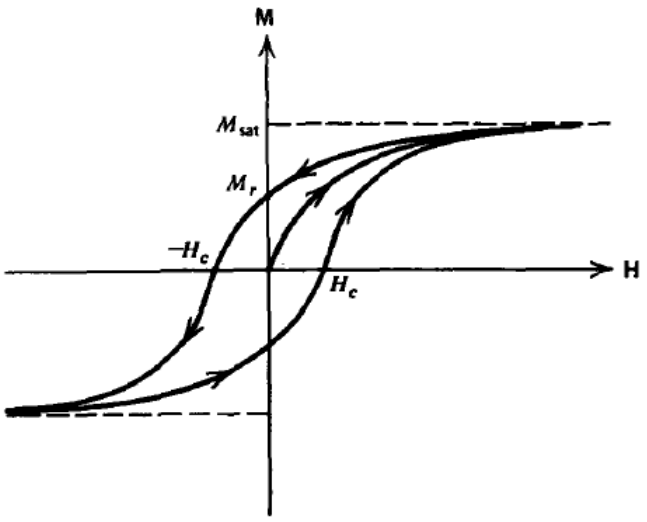

Figure 1.5. M-H curve for a ferromagnetic hard material. Figure from [17]

1.2.2. Formulation of the magnetic stress tensor using thermodynamic relations

We start from first law of thermodynamics:

$$\delta Q - \delta W = dU' \tag{1.6}$$

where δQ is the heat change, δW is the work done and the U' is the internal energy per unit mass. For a reversible process:

$$\delta Q = TdS' \tag{1.7}$$

where S' is the entropy change per unit mass and the Helmholtz Free Energy F' is given as

$$F' = U' - TS'$$

$$dF' = dU' - TdS' - S'dT \tag{1.8}$$

$$dF' = -\delta W - S'dT \tag{1.9}$$

$$\tag{1.10}$$

so in an isothermal case one can write $(dF')_T = -\delta W$ The work done can also be expressed as

$$\delta W = \underbrace{pdv}_{\text{thermodynamic work}} \underbrace{- d(v \int HdB)}_{\text{magnetic work}} \tag{1.11}$$

$$= (p - \int HdB)dv - vHdB \tag{1.12}$$

where $(v = \rho^{-1}(m^3/kg))$. So substituting (1.12) into (1.9) we obtain

$$dF' = -(p - \int HdB)dv + vHdB - S'dT \tag{1.13}$$

We can see a functional dependence exists that can be shown as $F' = F'(v, T, B)$ which under the absence of magnetic field($\mathbf{H}$=0), becomes

$$dF' = -pdv - S'dT \tag{1.14}$$

When there is no magnetic field, one can easily say that the free energy is a function of specific volume and temperature, that is, $F' = F'(v, T, 0)$ so we can write the total differential as

$$dF'(v,T,0) = \underbrace{\left(\frac{\partial F'}{\partial v}\right)_T}_{-p} dv + \underbrace{\left(\frac{\partial F'}{\partial v}\right)_v}_{-S'} dT \tag{1.15}$$

So when fields are absent, pressure and entropy are only dependent on the free energy. If we work with free energy per unit volume denoted F,

$$\begin{aligned} F' &= vF \\ dF' &= vdF + Fdv \end{aligned} \tag{1.16}$$

The thermodynamic pressure p can be formulated in terms of F that is the Helmholtz free energy per unit volume as

$$\left[\frac{\partial(vF)}{\partial v}\right]_T = -p \tag{1.17}$$

so that $p = p(\rho, T)$.

If we insert (1.16) into (1.13), we obtain the following relation under constant volume and constant temperature.

$$dF = HdB \tag{1.18}$$

This expression relates the thermodynamic free energy to the magnetostatic energy density.

1.2.2.1. Isothermal Magnetization at Constant Volume. Using the thermodynamic relations derived in the previous section, we can write

$$-(dF)_T = \delta W = -HdB \tag{1.19}$$

Integrating (1.19) at constant temperature we obtain

$$\begin{aligned} F(\rho, T, B) &= \left(\int_0^B HdB \right)_{\rho,T} + F_0(\rho, T) \\ F(\rho, T, H) &= F_0(\rho, T) + HB - \left(\int_0^H BdH \right)_{\rho,T} \end{aligned} \tag{1.20}$$

1.2.2.2. Isothermal Deformation. Let the fluid be deformed by an infinitesimal displacement vector ξ which is not necessarily normal to the plane so the displacement is $\delta a = \mathbf{n} \cdot \xi$. To obtain a magnetic fluid stress tensor, $\mathcal{T}'_m$, we can express the work done on the system as

$$\begin{aligned} \delta W &= -\mathbf{n} \cdot \mathcal{T}'_{\mathbf{m}} \cdot \xi \\ \delta W &= -d(Fa)_T = -Fda - adF_T \end{aligned} \tag{1.21}$$

where Fa is the free energy per unit area. An expression for dF_T can be obtained using (1.20) and mass conservation

$$dF_T = \left(\frac{\partial F_0}{\partial v} \right)_T dv + HdB - \int_0^H \left(\frac{dB}{dv} \right)_{H,T} dvdH \tag{1.22}$$

Using (1.21) we can write the stress tensor $\mathcal{T}'_m$ as

$$\mathcal{T}'_m = \left\{ \left(\frac{\partial (vF_0)}{\partial v} \right)_T - \int_0^H \left(\frac{\partial (vB)}{\partial v} \right)_{H,T} dH \right\} \mathcal{I} + \mathbf{BH} \tag{1.23}$$

The stress tensor is therefore symmetric since $\mathbf{BH} = \mathbf{HB}$ and $\mathcal{I}^T = \mathcal{I}$. The first term of the tensor represents the pressure ($-p_0(\rho, T)$). The second term can be rewritten using the constitutive relationship, $\mathbf{B} = \mu_0(\mathbf{H}+\mathbf{M})$ so the tensor becomes $\mathcal{T}_m = \mathcal{T}'_m + p(\rho, T)\mathcal{I}$ where

$$\mathcal{T}_m = -\left\{\int_0^H \left(\frac{\partial(vM)}{\partial v}\right) dH + \frac{1}{2}\mu_0 H^2\right\}\mathcal{I} + \mathbf{BH} \tag{1.24}$$

which at constant specific volume reduces to the Maxwell stress tensor.

1.3. Taylor-Couette Flows

The rotational flow between two concentric cylinders known as Taylor-Couette flow is a classical flow problem in fluid mechanics. Taylor-Couette devices are used as mixing devices in applications such as catalytic chemical reactors, rotating filtration devices and bioreactors [18–20]. Centrifugal effects generated by these devices are also needed to obtain stable suspensions of nano-sized particles in a solvent [21]. Transport phenomena in Taylor-Couette flows are also investigated widely in the literature. As stated above, in nanofluid studies, Taylor-Couette flow is a proposed method of nanofluid preparation, so stability studies play an important role. The Buongiorno model explained in [22] for the transport equations of nanofluids are mostly applied in the literature. Lopez *et al.* [23] worked on a single phase Newtonian fluid in a Taylor-Couette geometry, considering temperature dependant density so that centrifugal buoyancy is a significant body force in the momentum equation. They investigate the flow regimes transitions as a function of radial temperature gradient. Azaditalab *et al.* [24] worked numerically on skin friction reduction induced by nanofluid suspension on Taylor-Couette geometry. Taylor-Couette is known to have multiple stages of transition from laminar to turbulent regimes and have been subject to many theoretical and experimental investigations in the literature [25]. Andereck *et al.* [26] conducted Taylor-Couette flow experiment to reveal the different transition modes from laminar to

turbulent stages. For the gap ratios used in this study, Table 1.2 summarizes the measured Taylor number ranges for intermediate transition stages when the outer cylinder is stationary. The primary transition from Couette Flow (CF) to Taylor Vortex Flow

Table 1.2. Taylor number (Ta) ranges for intermediate transition stages [24, 26]. (The values are given for gap ratios(r_1/r_2) of 0.3 and 0.9.)

Flow regime	$r_1/r_2 = 0.3$	$r_1/r_2 = 0.9$
Couette flow	Ta< 140.5	Ta< 30.67
Taylor vortex flow	140.5 <Ta< 210.8	30.67 <Ta< 46
Wavy vortex flow	210.8 <Ta< 1558.1	46 <Ta< 340
Modulated wavy vortices	1558.1 <Ta< 2108	340 <Ta< 460
Turbulent Taylor vortices	2108 <Ta	460 <Ta

(TVF) was studied both experimentally and numerically by Taylor in his benchmark study [25]. Fasel *et al.* [27] conducted a flow analysis using finite difference technique for wide gap at supercritical Taylor numbers to investigate in more detail the axisymmetric Taylor vortex flow regime. Jones conducted stability analyses for the transition from Taylor vortex flow to wavy vortex flow where stationary axisymmetric Taylor vortices were used as the basic state and non-axisymmetric perturbations were imposed in the small-gap limit [28] and for a wider range of gap ratios [29] to investigate the onset of wavy vortex flow. Modulated Taylor-Couette flow was investigated by Jones and Barenghi [30], where they consider sinusoidally varying rotational frequencies of the cylinders. Modulated Taylor vortices have also been studied by Coughlin both analytically [31] and numerically [32].

In most of the publications in the literature, the transition from CF to TVF and to further flow regimes has been studied extensively for isothermal cases. There are also studies investigating this primary instability under the effect of radial temperature [23, 33, 34] and concentration gradients [21]. The first major study on Taylor-Couette stability under magnetic effects was done by Niklas [35] where an equation of

motion was derived for a ferrofluid in Taylor-Couette flow with magnetic field dependent rotational viscosity and the effects of magnetic fields applied in different directions were discussed. The work was later extended to account for non-axisymmetric perturbations. [36] Stiles [37] considered an isothermal Taylor-Couette problem with axial magnetic field and developed analytical expressions for the narrow gap case that relate the criticial Taylor number to axial magnetic field strength. Odenbach [38] made an experimental study of magnetized Taylor-Couette flow with azimuthal magnetic field resulting from an alternating surface current flowing along the inner cylinder in the axial direction. Stiles *et al.* [39] investigates the non-isothermal case of a ferrofluid Taylor-Couette flow with a radial temperature difference and radial magnetization, to report significant drop in critical Taylor number with small temperature changes. In this study, we examine the instability mechanisms of non-isothermal Taylor-Couette flow of a ferrofluid under the action of an azimuthal external magnetic field with radial temperature gradients. The main purpose of this study is to underline the effects of azimuthal magnetic field strength, radial temperature difference, ferroparticle concentration and size on the stability of Couette flow. The gap effects on the stability are also demonstrated.

1.4. Objectives and Originality

The literature survey presented in the previous sections underline that a study that focuses on the thermomagnetic effects on the stability of Taylor-Couette flows is lacking. Non-Isothermal Taylor-Couette flow of a ferrofluid is investigated in this study. The magnetic field of an axial DC current, which only has azimuthal component that decays with radial distance, is accounted to underline and discuss magnetic field effects. Magnetocaloric heat storage due to the temperature dependence of the magnetization field and magnetic relaxation effects are also taken into account. These considerations allow the investigation of the combined coupled effects of the thermal non-uniformity with magnetic field.

2. MATHEMATICAL FORMULATION

2.1. Governing Equations and Boundary Conditions

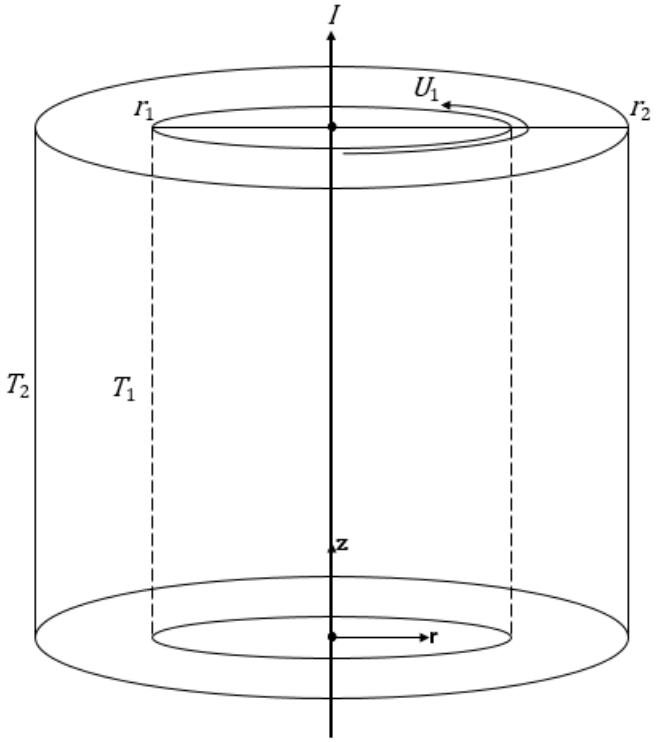

Figure 2.1. Flow geometry

The flow geometry is given in Figure 2.1, and represents Taylor-Couette ferrofluid flow under radial temperature gradient and with a line current I flowing along the z-axis. The unit normal vectors in the radial and axial directions are given by $\mathbf{r}$ and $\mathbf{z}$, respectively. The inner cylinder of radius r_1 is rotating with a velocity $U = U_1$ while the outer cylinder of radius r_2 is stationary. The inner and outer walls are kept at constant temperatures $T = T_1$ and $T = T_2$, respectively. The line current results in an azimuthal magnetic field decaying radially, making the problem similar to that studied experimentally by Odenbach. [38] The governing mass, linear and angular momentum, energy, magnetic relaxation and magnetostatic equations are given respectively

as follows,

$$\nabla \cdot \mathbf{u} = 0 \tag{2.1}$$

$$\rho_f \frac{D\mathbf{u}}{Dt} = -\nabla p + \eta \nabla^2 \mathbf{u} + \mu_0 (\mathbf{M} \cdot \nabla)\mathbf{H} + \frac{1}{2\tau_s} \nabla \times \left(\mathbf{S} - \frac{J}{2} \nabla \times \mathbf{u} \right) + \rho \frac{u_\theta^2}{r} \mathbf{r} \tag{2.2}$$

$$\frac{D\mathbf{S}}{Dt} = \mu_0 (\mathbf{M} \times \mathbf{H}) - \frac{1}{\tau_s} \left(\mathbf{S} - \frac{J}{2} \nabla \times \mathbf{u} \right) + \eta' \nabla^2 \mathbf{S} \tag{2.3}$$

$$\left(\rho c - \mu_0 \mathbf{H} \cdot \frac{\partial \mathbf{M}}{\partial T} \right) \frac{DT}{Dt} = k_f \nabla^2 T \tag{2.4}$$

$$\frac{D\mathbf{M}}{Dt} = \frac{1}{J} (\mathbf{S} \times \mathbf{M}) - \frac{1}{\tau_B} \left(\mathbf{M} - M_{eq} \frac{\mathbf{H}}{H} \right) \tag{2.5}$$

$$\nabla \cdot \mathbf{B} = 0 \tag{2.6}$$

$$\mathbf{B} = \mu_0 (\mathbf{M} + \mathbf{H}) \tag{2.7}$$

where $\frac{D}{Dt} = \frac{\partial}{\partial t} + (\mathbf{u} \cdot \nabla)$ is the material derivative. In this formulation t denotes the time, $\mathbf{u} = [u, v, w]$ is the velocity vector with cylindrical components, p is the pressure field, $\mathbf{S}$ is the internal angular momentum vector, T is the temperature field. $\mathbf{H}$ and $\mathbf{M}$ are the magnetic and magnetization field vectors respectively. The base fluid density is represented by ρ_f, η is the magnetic field dependent dynamic viscosity, μ_0 is the magnetic permeability of free space, ρc is the heat capacity, k_f is the thermal

conductivity of the base fluid, ϕ is the volume fraction of magnetic particles to base fluid, which is assumed to be independent of space. The characteristic time scale for mass diffusion is up to 5 degrees of magnitude longer than the characteristic time scale for momentum diffusion. Their ratio is the Schmidt number ($\mathrm{Sc} = \eta/\rho D_B$ where D_B is the Brownian diffusivity) and it is typically around 10^5 for a water based ferrofluid and for the temperature and particle size values used in this study. One can therefore treat the fluid as pure since mass diffusion needs a much longer time to evolve. [40–43] Brownian relaxation time of the magnetic particles is denoted by τ_B. The parameters η', τ_s and J represent the spin viscosity, spin relaxation time and the volume density of the moment of inertia of the magnetic particles, respectively. The last term on the right hand side of Equation (2.2) represents the centrifugal force in the radial direction where the density, ρ, is given in accordance with the Boussinesq approximation [44], by the expression;

$$\rho = \phi\rho_p + (1-\phi)\rho_f(1-\beta(T-T_{ref})) \tag{2.8}$$

where β is the thermal coefficient of water and ρ_p is the density of the nanoparticle. The following assumptions can be made under most conditions, which are also supported in Refs. [6, 45]: the evolution of the internal angular momentum is time independent and the spin viscosity (i.e. spin diffusion) is negligibly small due to the small size of particles. Under these assumptions Equation (2.3) reduces to

$$\mathbf{S} - \frac{J}{2}\nabla \times \mathbf{u} = \mu_0\tau_s(\mathbf{M} \times \mathbf{H}) \tag{2.9}$$

Equation (2.9) suggests that in the absence of magnetic torque ($\mathbf{M} \times \mathbf{H}$), the internal angular momentum ($\mathbf{S}$) is equal to the rotation of solvent ($I(\nabla \times \mathbf{u})/2$). Using Equation (2.9) we can simplify the linear momentum equation in Equation (2.2) as

$$\rho_f \frac{D\mathbf{u}}{Dt} = -\nabla p + \eta\nabla^2\mathbf{u} + \mu_0(\mathbf{M}\cdot\nabla)\mathbf{H} + \frac{\mu_0}{2}\nabla \times (\mathbf{M} \times \mathbf{H}) + \rho\frac{u_\theta^2}{r}\mathbf{r} \tag{2.10}$$

Similarly, taking $\tau_s = \rho_p d^2/60\eta$ and $J = \rho_p \phi d^2/10$, we can rewrite the magnetic relaxation equation in Equation (2.5) as

$$\frac{D\mathbf{M}}{Dt} = \frac{1}{2}(\nabla \times \mathbf{u}) \times \mathbf{M} + \frac{\mu_0}{6\eta\phi}(\mathbf{M} \times \mathbf{H}) \times \mathbf{M} - \frac{1}{\tau_B}\left(\mathbf{M} - M_{eq}\frac{\mathbf{H}}{H}\right) \tag{2.11}$$

So the set of governing equations for this system are Equations (2.10), (2.4) and (2.11) along with (2.1) and (2.6).

2.2. Magnetic Field Definitions

The problem studied in this paper considers a magnetic field resulting from external current. The general form of the Ampere's Law is given as,

$$\nabla \times \mathbf{H}_0 = \mathbf{J}_e + \mathbf{J}_i \tag{2.12}$$

with the external current, $\mathbf{J}_e$ and the induced current $\mathbf{J}_i = \sigma_c(\mathbf{E} + \mathbf{u} \times \mathbf{B})$ where σ_c is the conductivity of the medium and $\mathbf{H}_0$ is the external magnetic field. The ferrofluid is assumed to be non-conductive ($\sigma_c = 0$), hence there are no induced currents ($\mathbf{J}_i = 0$). If we consider a magnetic field due to a permanent magnet, this leads to a curl-free magnetic field ($\nabla \times \mathbf{H}_0 = 0$), as commonly used in the ferrofluid literature. In our problem, however, Equation (2.12) reduces to $\nabla \times \mathbf{H}_0 = \mathbf{J}_e$. The azimuthal magnetic field resulting from an external axial current $I\mathbf{z}$ can be formulated by integrating $\nabla \times \mathbf{H}_0 = \mathbf{J}_e$ using Stokes' Law, as

$$\oint_L \mathbf{H}_0 \cdot \mathbf{dl} = \int \mathbf{J}_e \cdot \mathbf{dA} = I \tag{2.13}$$

from which it can be deduced that $H_\theta = I/2\pi r$ with $r \in (0, \infty)$. In the absence of induced or free surface currents, the tangential component of $\mathbf{H}_0$ is continuous across the radial boundaries of the fluid domain. For the linear stability problem,

the perturbations in the local magnetic field $\mathbf{H}$ are neglected such that $\mathbf{H} = \mathbf{H}_0$. With the parameter ranges covered in this study, the equilibrium susceptibility, which is the ratio of equilibrium magnetization to external magnetic field strength, is at most $O(10^{-2})$. Therefore the $O((M' \cdot H_0)/L)$ terms will be dominant over the $O((M_0 \cdot H')/L)$ terms, where the symbols with prime denote perturbations in the corresponding fields and L is a length scale. Then the perturbations in local magnetic field H' may be neglected as also explained in [35, 46]. Approximating the local field $\mathbf{H}$ with external field $\mathbf{H}_0$ allows to define a divergence free magnetization field in the perturbed state as the form of the magnetic field determined by (2.13) satisfies $\nabla \cdot \mathbf{H}_0 = 0$ which leads to $\nabla \cdot \mathbf{M} = 0$ due to Equations (2.6) and (2.7).

The equilibrium magnetization of the fluid aligned with the external magnetic field is denoted by M_{eq}, and is governed by the Langevin relation given by,

$$\begin{aligned} M_{eq} &= \phi M_d \mathcal{L}(\alpha_L) \\ &= \phi M_d (\coth(\alpha_L) - \frac{1}{\alpha_L}) \end{aligned} \tag{2.14}$$

where M_d is the bulk magnetization of the magnetic particle and $\mathcal{L}(\alpha_L)$ is the Langevin function where $\alpha_L = \frac{\pi}{6} \frac{\mu_0 d^3 M_d H}{k_B T}$ is the local Langevin parameter. [6] In this expression d represents the nanoparticle diameter and k_B is the Boltzmann constant. The magnetic field dependent viscosity, η, is given in non-dimensional form as η^* which can be expressed as, [47]

$$\eta^* = \frac{\eta}{\eta_0} = \frac{3}{2}\phi \frac{\alpha_L - \tanh(\alpha_L)}{\alpha_L + \tanh(\alpha_L)} \tag{2.15}$$

where η_0 is the dynamic viscosity of the base fluid.

2.3. Non-dimensionalization and Perturbation Equations

All of the variables in the above system of Equations (2.10), (2.4) and (2.11) are non-dimensionalized by introducing the following non-dimensional variables,

$$r^* = \frac{r}{r_2} = \frac{x(1-\zeta)+(1+\zeta)}{2} \qquad x = \frac{2r-(r_1+r_2)}{\Delta r}$$

$$t^* = \frac{t\eta}{\Delta r \rho_f} \qquad \mathbf{u}^* = \frac{\mathbf{u}}{U_1} \qquad p^* = \frac{pr_2}{U_1\eta} \qquad T^* = \frac{T-T_1}{T_2-T_1} \tag{2.16}$$

$$\mathbf{M}^* = \frac{\mathbf{M}}{M_d} \qquad H^* = \frac{H_\theta}{H_0} = \frac{1}{r^*}$$

where $\Delta r = r_2 - r_1$. The magnetic field strength scale, H_0, is the value of magnetic field strength at the outer cylinder ($H_0 = I/2\pi r_2$). The temperature dependent density given in (2.8) is also scaled with ρ_f to give the non-dimensional density ρ^* as,

$$\rho^* = \frac{\rho}{\rho_f} = \phi\left(\frac{\rho_p}{\rho_f}\right) + (1-\phi)(1-c_{\rho,T}T^*) \tag{2.17}$$

The nondimensional form of the component equations become

$$\frac{\partial u^*}{\partial t^*} + \mathrm{Re}\left(u^*\frac{\partial u^*}{\partial r^*} + w^*\frac{\partial u^*}{\partial z^*}\right) = -\frac{\partial p^*}{\partial r^*} + \left(\frac{\partial^2 u^*}{\partial r^{*2}} + \frac{1}{r^*}\frac{\partial u^*}{\partial r^*} - \frac{u^*}{r^{*2}} + \frac{\partial^2 u^*}{\partial z^{*2}}\right) + \mathrm{Re}\frac{\rho^* v^{*2}}{r^*} - \frac{\mathrm{R_M}}{\mathrm{Re}}\frac{M_\theta^* H^*}{r^*} \tag{2.18}$$

$$\frac{\partial v^*}{\partial t^*} + \mathrm{Re}\left(u^*\frac{\partial v^*}{\partial r^*} + w^*\frac{\partial v^*}{\partial z^*} + \frac{u^* v^*}{r^*}\right) = \left(\frac{\partial^2 v^*}{\partial r^{*2}} + \frac{1}{r^*}\frac{\partial v^*}{\partial r^*} - \frac{v^*}{r^{*2}} + \frac{\partial^2 v^*}{\partial z^{*2}}\right) \tag{2.19}$$

$$\frac{\partial w^*}{\partial t^*} + \mathrm{Re}\left(u^*\frac{\partial w^*}{\partial r^*} + w^*\frac{\partial w^*}{\partial z^*}\right) = -\frac{\partial p^*}{\partial z^*} + \left(\frac{\partial^2 w^*}{\partial r^{*2}} + \frac{1}{r^*}\frac{\partial w^*}{\partial r^*} + \frac{\partial^2 w^*}{\partial z^{*2}}\right) \tag{2.20}$$

$$\frac{\partial T^*}{\partial t^*} + \mathrm{Re}\left(u^*\frac{\partial T^*}{\partial r^*} + w^*\frac{\partial T^*}{\partial z^*}\right) = \frac{1}{\mathrm{Pr}}\left(\frac{\partial^2 T^*}{\partial r^{*2}} + \frac{1}{r^*}\frac{\partial T^*}{\partial r^*} + \frac{\partial^2 T^*}{\partial z^{*2}}\right) + \kappa\left[\frac{\partial M_\theta^*}{\partial t} + \mathrm{Re}\left(u^*\frac{\partial M_\theta^*}{\partial r^*} + w^*\frac{\partial M_\theta^*}{\partial z^*}\right)\right] \tag{2.21}$$

$$\frac{\partial M_r^*}{\partial t} + \mathrm{Re}\left(u^*\frac{\partial M_r^*}{\partial r^*} + w^*\frac{\partial M_r^*}{\partial z^*}\right) = \frac{1}{2}\mathrm{Re}\left[\left(\frac{\partial u^*}{\partial z^*} - \frac{\partial w^*}{\partial r^*}\right)M_z^* - \frac{1}{r^*}\frac{\partial (r^* v^*)}{\partial r^*}M_\theta^*\right] - \frac{\mathrm{R_M}}{6\phi}M_r^* M_\theta^* H^* - \mathrm{R_H}M_r^* \tag{2.22}$$

$$\frac{\partial M_\theta^*}{\partial t} + \mathrm{Re}\left(u^*\frac{\partial M_\theta^*}{\partial r^*} + w^*\frac{\partial M_\theta^*}{\partial z^*}\right) = \frac{1}{2}\mathrm{Re}\left[\frac{1}{r^*}\frac{\partial (r^* v^*)}{\partial r^*}M_r^* + \frac{\partial v^*}{\partial z^*}M_z^*\right] - \frac{\mathrm{R_M}}{6\phi}(M_r^{*2} + M_z^{*2})H^* - \mathrm{R_H}(M_\theta^* - \phi\mathcal{L}(\alpha_L)) \tag{2.23}$$

$$\frac{\partial M_z^*}{\partial t} + \mathrm{Re}\left(u^*\frac{\partial M_z^*}{\partial r^*} + w^*\frac{\partial M_z^*}{\partial z^*}\right) = \frac{1}{2}\mathrm{Re}\left[\left(\frac{\partial w^*}{\partial r^*} - \frac{\partial u^*}{\partial z^*}\right)M_r^* - \frac{\partial v^*}{\partial z^*}M_\theta^*\right] - \frac{\mathrm{R_M}}{6\phi}M_z^* M_\theta^* H^* - \mathrm{R_H}M_z^* \tag{2.24}$$

For the non-linear analysis using COMSOL, these set of equations are solved directly. For the linear stability analysis, one must obtain basic state solutions and dissect the dependent variables into base state and perturbed state. The brevity of linear analysis comes from neglecting the terms where the perturbed states are multiplied since perturbations are assumed to be infinitesimal and their nonlinear effects can be neglected.

The basic flow state is the Couette flow which represents the 1-D steady state solution of the system of Equations (2.1)-(2.6) and is written in terms of the flow

variables as,

$$\mathbf{u}^* = (0, V(r^*), 0) \qquad T^* = \Theta(r^*) \qquad \mathbf{M}^* = (0, M_0, 0) \tag{2.25}$$

Using $v^* = 1, T^* = 0$ at $r^* = \zeta$ and $v^* = 0, T^* = 1$ at $r^* = 1$ as boundary conditions, the functions in the above basic state solution (2.25) can be expressed as,

$$V(r^*) = A\left(r^* - \frac{1}{r^*}\right) \qquad \text{with} \qquad A = \frac{\zeta}{\zeta^2 - 1} \tag{2.26}$$

$$\Theta(r^*) = 1 - \frac{log(r^*)}{log(\zeta)} \tag{2.27}$$

$$M_0 = \phi\mathcal{L}(\alpha_L) \qquad \text{with} \qquad \alpha_L = \frac{c_M H^*}{c_T\Theta + c_{T2}} \tag{2.28}$$

where the gap ratio of the concentric cylinders is given as $\zeta = r_1/r_2$, $c_M = \frac{\pi}{6}\mu_0 d^3 M_d H_0$, $c_T = k_B(T_2 - T_1)$ and $c_{T2} = k_B T_1$.

After the basic state is derived, infinitesimal perturbations are imposed on the basic flow to investigate the critical Taylor number for the transition from CF to TVF, in the following form,

$$\begin{aligned}
\mathbf{u}^* &= (0, V(r^*), 0) + (\hat{u}_r, \hat{u}_\theta, \hat{u}_z)(x)e^{\sigma t^* + ikz^*} \\
p^* &= \hat{p}(x)e^{\sigma t^* + ikz^*} \\
T^* &= \Theta(r^*) + \hat{T}(x)e^{\sigma t^* + ikz^*} \\
\mathbf{M}^* &= (0, M_0, 0) + (\hat{M}_r, \hat{M}_\theta, \hat{M}_z)(x)e^{\sigma t^* + ikz^*}
\end{aligned} \tag{2.29}$$

where σ is the dimensionless amplification factor and k is the dimensionless wavenumber. The variables with hat ($\hat{}$) symbol denote the related perturbation amplitudes. The temperature dependent density given in (2.8) is also scaled with ρ_f to give the non-dimensional density ρ^* as,

$$\rho^* = \frac{\rho}{\rho_f} = \phi\left(\frac{\rho_p}{\rho_f}\right) + (1-\phi)(1 - c_{\rho,T}T^*) \tag{2.30}$$

and decomposed into a basic ($\bar{\rho}$) and a perturbed state (ρ') resulting from the perturbations in temperature (T') with T_{ref} taken as T_1, which is finally expressed as,

$$\rho^* = \underbrace{\phi\left(\frac{\rho_p}{\rho_f}\right) + (1-\phi)(1 - c_{\rho,T}\Theta)}_{\bar{\rho}} - \underbrace{(1-\phi)c_{\rho,T}T'}_{\rho'} \tag{2.31}$$

where $c_{\rho,T} = \beta(T_2 - T_1)$. The term underbraced as $\bar{\rho}$ in (2.31) represents the variation of the density in the basic state as a function of temperature which is mostly neglected in the literature. The linear analysis shows that accounting for this variation results in a rise in the critical Taylor number which is also confirmed by the solution of the full nonlinear system of equations. Therefore we choose to include this term for the rest of the calculations presented in this paper.

When the variable expressions in Equation (2.29) and Equation (2.31) are substituted into Equations (2.18)-(2.24), the nonlinear terms are neglected, and the perturbation amplitudes $\hat{p}$, $\hat{u}_z$ and $\hat{M}_z$ are eliminated using the divergence-free properties of velocity and magnetization fields, we finally obtain the following set of linear ordinary differential equations for the perturbation amplitudes,

$$\begin{aligned}\sigma(DD^* - k^2)\hat{u}_{Re} =& \eta^*(DD^* - k^2)^2\hat{u}_{Re} \\ &+ k^2\left[\frac{\mathrm{R}_M}{\mathrm{Re}}\left(\frac{1-\zeta}{r^*}\right)H^*\hat{M}_\theta - \frac{\zeta}{r^*}\mathrm{Ta}^2 V(2\bar{\rho}\hat{u}_\theta - \rho' V)\right]\end{aligned} \tag{2.32}$$

$$\sigma\hat{u}_\theta = -2(1-\zeta)A\hat{u}_{Re} + \eta^*(DD^* - k^2)\hat{u}_\theta \tag{2.33}$$

$$\sigma \mathrm{Pr}\hat{T} = -\mathrm{Pr}D\Theta\hat{u}_{Re} + (D^*D - k^2)\hat{T} + \kappa\mathrm{Pr}(\mathrm{Re}(1-\zeta)A\hat{M}_r - \mathrm{R}_H\hat{M}_\theta) \tag{2.34}$$

$$\begin{aligned}\sigma\left(\frac{1-\zeta}{r^*}\right)\hat{M}_r = \frac{\mathrm{Re}}{2}&(M_0(DD^* - k^2) + DM_0D^*)\hat{u}_\theta \\ &+ \mathrm{Re}\left(\frac{1-\zeta}{r^*}\right)\left(DM_0 - \left(\frac{1-\zeta}{r^*}\right)M_0 + M_0D\right)\hat{u}_\theta \\ &+ \mathrm{Re}\left[(1-\zeta)AD + \left(\frac{1-\zeta}{r^*}\right)\left(DV - \left(\frac{1-\zeta}{r^*}\right)V + VD\right)\right]\hat{M}_\theta \\ &+ \left(DF_{MH} - \left(\frac{1-\zeta}{r^*}\right)F_{MH}\right)\hat{M}_r\end{aligned} \tag{2.35}$$

$$\sigma\hat{M}_\theta = -DM_0\hat{u}_{Re} + \mathrm{Re}(1-\zeta)\left(A - \frac{V}{r^*}\right)\hat{M}_r - \mathrm{R}_H\hat{M}_\theta \tag{2.36}$$

The operator symbols and non-dimensional parameters appearing in Equations (2.32)-(2.36) are given as follows,

$$\begin{gathered} D = 2\frac{d}{dx} \qquad D^* = 2\frac{d}{dx} + \frac{1-\zeta}{r^*} \\ \mathrm{Re} = \frac{\rho_f U_1 \Delta r}{\eta_0} \qquad \mathrm{Re}^2(1-\zeta) = \mathrm{Ta}^2\zeta \qquad \hat{u}_{Re} = \mathrm{Re}\hat{u}_r \\ \mathrm{Pr} = \frac{\eta_0 c}{k_f} \qquad \mathrm{R}_M = \frac{\mu_0\rho_f\Delta r^2 M_d H_0}{\eta_0^2} \qquad \kappa = \frac{\mu_0 M_d H_0}{\rho c(T_2 - T_1)} \\ \mathrm{R}_H = \frac{\rho_f \Delta r^2}{\eta_0 \tau_B} \qquad F_{MH} = \frac{\mathrm{R}_M}{6\eta\phi}M_0H_0 + \mathrm{R}_H \end{gathered} \tag{2.37}$$

where Re is the Reynolds number, Pr is the Prandtl number and the definition of the Taylor number (Ta) follows the definition in Walowit. [33] The boundary conditions for the perturbation amplitudes at $x = \pm 1$ are Dirichlet and clamped conditions given

by,

$$\hat{u}_{Re} = D\hat{u}_{Re} = \hat{u}_{\theta} = \hat{T} = 0 \tag{2.38}$$

In alignment with $\nabla \cdot \mathbf{M} = 0$, the normal component of $\mathbf{B}$ must be continuous at the boundaries therefore the perturbation amplitudes of the magnetization at the boundary must also be zero and they are given as,

$$\hat{M}_r = \hat{M}_{\theta} = 0 \tag{2.39}$$

3. NUMERICAL METHOD AND VALIDATION

3.1. Linear Stability

The system of linear stability equations (2.32)-(2.36), constitutes an eigenvalue problem of the form $\mathbf{Ax} = \sigma\mathbf{Bx}$ which can effectively be solved by Galerkin weighted residual methods. Generally, these methods are trying to solve a linear operator $L(u) = 0$ by assuming trial functions of known analytic functions, $\phi(x)$, in the form

$$u_a(\mathbf{x}, t) = u_0(\mathbf{x}, t) + \sum_{j=1}^{N} a_j(t)\phi_j(\mathbf{x}, t) \tag{3.1}$$

so that $L(u_a) = R$ where R is the residual. The set of coefficients, a_j, are to be obtained by taking the inner product of the residual with a weight function, $w(x)$, and setting that equal to 0, at N sampling points [48].

$$(R, w_k(\mathbf{x})) = 0, \qquad k = 1, ..., N, \tag{3.2}$$

In the domain $[-1, 1]$, the inner product of two arbitrary functions f and g can be shown as

$$(f, g) = \int_{-1}^{1} f(x)g(x)dx \tag{3.3}$$

The inner product may also be calculated in a discrete sense.

$$(f, g) = \sum_{i=1}^{N} f_i g_i \tag{3.4}$$

In Chebyshev collocation, the trial functions are composed of Chebyshev polynomials of the first kind and the weight function is the Dirac function so the inner product

reduces to evaluating the residual at sample points, like the extrema of the Chebyshev polynomials.

Applying the above method to our problem, the variables $\hat{u}_{Re}, \hat{u}_\theta, \hat{T}, \hat{M}_r, \hat{M}_\theta$, are assigned trial functions in the form of Chebyshev polynomials. Functions `chebdif.m` and `cheb4c.m` [49] were utilized to solve the system using MATLAB, in which the differentiation matrices $D_{m,n}$ are constructed as follows,

$$D^{(1)}_{m,n} = \begin{cases} \frac{c_m(-1)^{n+m}}{c_n(x_m - x_n)}, & n \neq m \\ -\frac{1}{2}\frac{x_m}{(1-x_m^2)}, & n = m \neq 1 \\ \frac{2(N-1)^2+1}{6}, & n = m = 1 \\ -\frac{2(N-1)^2+1}{6}, & n = m = N \end{cases}$$

where $c_1 = c_N = 2$, $c_2 = \ldots = c_{N-1} = 1$ and $D^{(l)} = \left(D^{(1)}\right)^l$. The interpolation points are the Chebyshev nodes of the second kind given as

$$x_m = sin\left(\frac{\pi(N+1-2m)}{2(N-1)}\right) \tag{3.5}$$

where $m = 1 \ldots N$ and N is the number of collocation points. After constructing the matrices based on Equations (2.32)-(2.36), the generalized eigenvalues are calculated using QZ-algorithm and the neutral stability curves are obtained in terms of the Taylor (Ta) and wavenumbers (k) where the real part of the leading eigenvalue is zero. In our calculations we observed that a value of $N = 100$ is sufficient to obtain numerical convergence with an accuracy of the order of 10^{-4}. For all the cases we studied, $\sigma_r = \sigma_i = 0$ was observed where $\sigma = \sigma_r + i\sigma_i$; which means the instability sets in cellular convection also known as Taylor vortices.

3.2. Nonlinear Stability

The nonlinear stability problem was solved in COMSOL using a Direct Numerical Simulation (DNS) approach. The set of equations (2.18)-(2.24) are solved directly in COMSOL. Since $\sigma_i = 0$, the instability is stationary rather than oscillatory in time and therefore stationary solvers have been used to solve the magnetic relaxation equation in 2D axisymmetric geometry. The axial length of the annulus is set using an aspect ratio of $\Gamma = L/h = 10$. The conditions in axial boundaries are set to be periodic in all variables. To observe the onset of cellular convection (i.e. Taylor vortices), we conducted parametric sweep starting from %50 of the critical Taylor number obtained from the linear analysis and increased until the vortices are clearly visible. The grid independence is reached after around 3×10^5 degrees of freedom and our simulation used a mesh with 341296 degrees of freedom (corresponding to 48552 quadratic elements). Figures 3.1 and 3.2 show the variation of the nondimensional kinetic energy (E_K) integrated over the $r-z$ plane ($\int_0^{\Gamma(1-\zeta)} \int_\zeta^1 \frac{u^{*2}}{2} dr^* dz^*$)) with respect to degrees of freedom of the finite element simulation and the resulting grid-independent mesh.

The linear stability solutions are tested with the stability results of Walowit [33] for isothermal and non-isothermal cases under radial temperature gradient in the absence of the magnetic field. Figure 3.3 shows the neutral curves for the onset of transition from CF to TVF, where the minimum points reveal the pairs of critical wavenumber and Taylor number, (k_{cr},Ta_{cr}), for each gap ratio, ζ. The results are in good agreement with the isothermal results of Walowit. [33]

Taylor [25] had observed that the critical values obtained from linear stability analysis agree well with experimental results, which points that a nonlinear analysis should give the same critical Taylor number for the transition from CF to TVF. This hypothesis is also validated with the numerical solution of the full system of equations using COMSOL. Figure 3.3 shows the streamline plots obtained using COMSOL which

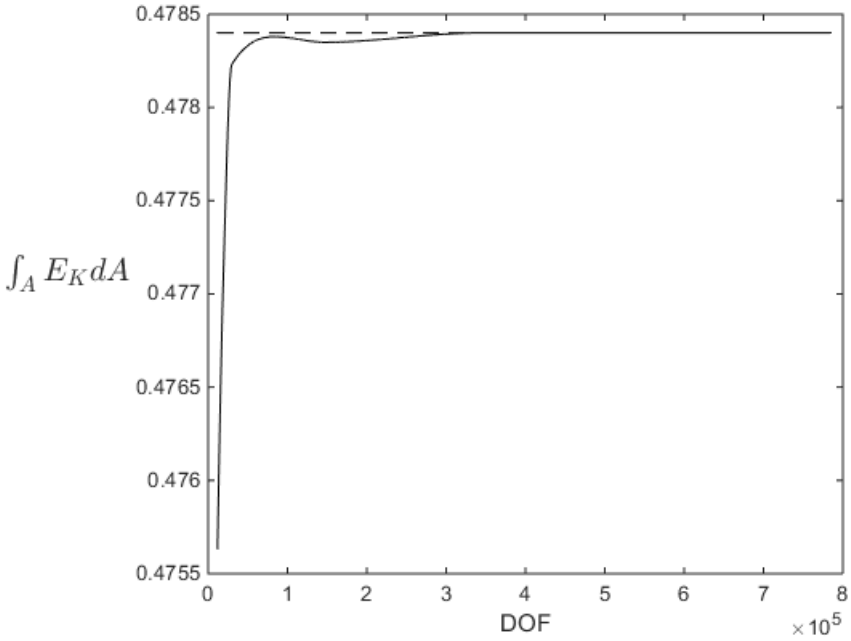

Figure 3.1. The convergence of the nondimensional kinetic energy integrated over the r-z plane with respect to degrees of freedom of the finite element simulation.

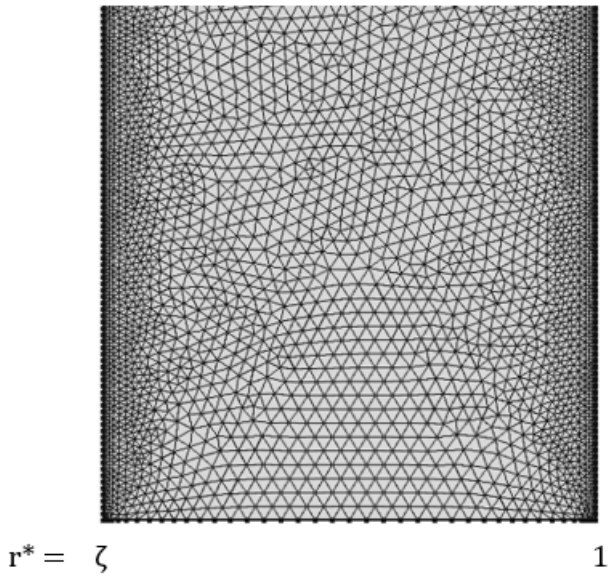

Figure 3.2. A screenshot of the mesh from the lower portion of the axisymmetric geometry.

verify the existence of Taylor vortices at Ta = 111.85. One can observe from Figure 3.3 that instabilities and flow bifurcation begins at earlier stages due to nonlinear effects

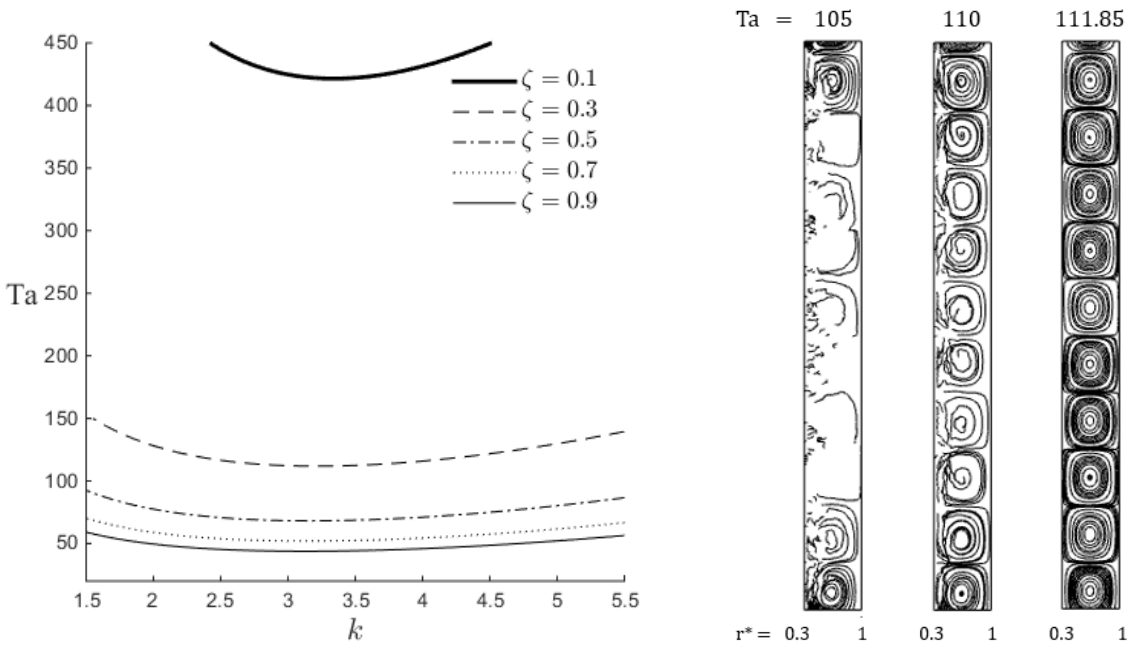

Figure 3.3. Neutral stability curves for isothermal flow with different gap ratios (left) Streamline plots from nonlinear study at $\zeta = 0.3$ (right)

however the settling of the Taylor Vortex Flow occurs at the critical Taylor number which is obtained from the linear analysis. The critical point in k-Ta space for $\zeta = 0.3$ is (3.217,111.85) in the corresponding neutral stability curve. Figure 3.3 illustrates also the effect of gap width on the stability of Couette flow. It can be observed that narrowing the gap width destabilizes the flow significantly, shifting the neutral stability curve downwards, which is also in agreement with the results in the literature. [25] The isothermal results and their validations are also gathered in Table 3.1.

To test the non-isothermal results, we use the values in Avramenko [21] for the parameter $c_{\rho,T}(= \beta(T_2 - T_1))$, which is a non-dimensional coefficient representing the density change due to temperature difference, and we demonstrate the effects of the inclusion of the basic state density variation $\bar{\rho}$ in Equation (2.31). Figure 3.4 shows the neutral stability curves and the resultant Taylor vortices for the non-isothermal case for the gap ratio $\zeta = 0.3$. We use a sample case from Avramenko's study ($c_{\rho,T} = 1$) to illustrate the effects of the variation of the density in the basic state. The critical Taylor

Table 3.1. Comparison of the isothermal results with those of Walowit [33]

ζ	This paper		Data of Walowit [33]	
	k_{cr}	Ta_{cr}	k_{cr}	Ta_{cr}
0.1	3.35	421.39	3.3	422.79
0.3	3.21	111.85	3.2	111.89
0.5	3.15	68.15	3.16	68.18
0.7	3.13	52.04	3.14	52.04
0.9	3.15	43.87	3.13	43.88

number for $c_{\rho,T} = 1$ is Ta = 91.9 without including the variation of the density in the basic state, while Ta = 94.6 is the critical value taking this variation into account, shown in the neutral curves in Figure 3.4 and the corresponding vortices. Table 3.2 compares the results at a gap ratio of $\zeta = 0.3$. The inclusion of the base state density variation reduces the destabilizing effect of the positive temperature gradient and reduces the stabilizing effect of the negative temperature gradient ($c_{\rho,T} < 0$).

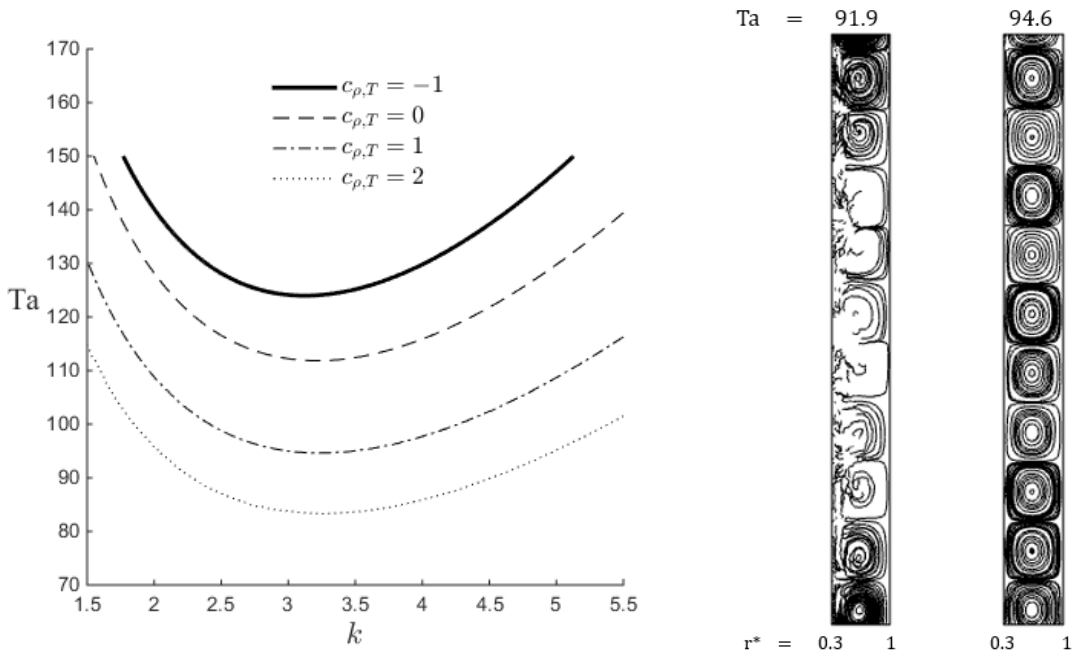

Figure 3.4. Neutral stability curves for nonisothermal flow with different values of the parameter $c_{\rho,T}$ at $\zeta = 0.3$ (left) Streamline plots for $c_{\rho,T} = 1$ at $\zeta = 0.3$ (right)

Table 3.2. Comparison of the non-isothermal critical values at gap ratio of $\zeta = 0.3$ with the results of Avramenko [21]

$c_{\rho,T}$	This paper		Data of Avramenko [21]	
	k_{cr}	Ta_{cr}	k_{cr}	Ta_{cr}
-1	3.14	123.98	3.02	152.79
1	3.23	94.63	3.231	91.9
2	3.25	83.31	3.245	79.76

The values of the parameter $c_{\rho,T}$ used in Ref. [21] correspond to very large values of ΔT if the value taken for β is that of water's (given in Table 4.1). Therefore the effect of $c_{\rho,T}$, which scales the density change in the fluid due to temperature difference, is magnified both in Ref. [21] and in Figure 3.4. Using the values in Table 4.1 and the values of ΔT studied later in this paper, the parameter $c_{\rho,T}$ ranges from -2.6×10^{-3} to 1.3×10^{-2}, which is relatively low compared to the values investigated by Avramenko *et al.* [21]. It can be concluded that an increase in the parameter $c_{\rho,T}$ destabilizes the flow. Higher values of $c_{\rho,T}$ point to a density decrease towards the outer wall which in turn favors flow bifurcation and vortical structures. [21] The non-dimensional critical wavenumber can also be deduced from the streamline plots by using the relation $\Gamma k_{cr} = \pi n_{vortex}$ where Γ is the aspect ratio and n_{vortex} is the number of vortices in the plots. [50] The streamline plots given in Figures 3.3 and 3.4 reveal that $k_{cr} \approx \pi$, which confirms the critical wavenumber in the neutral curves.

4. RESULTS AND DISCUSSION

To investigate the effects of azimuthal magnetic field strength, radial temperature difference and particle concentration and size on the stability of Couette flow in the presence of magnetic field, we choose a typical water-magnetite suspension with the thermophysical and magnetic properties given in Table 4.1. We conduct a parametrical study by changing the azimuthal magnetic field strength at the outer wall, H_0, the temperature difference, $\Delta T = T_2 - T_1$, the ferroparticle concentration ϕ and size d. Each of these dimensional parameters appear in different non-dimensional numbers defined in Equation (2.37). The parametrical study is conducted with respect to these dimensional parameters with values chosen from practical ranges to demonstrate the realistic effects which could be verified with experiments. The gap effects are considered for a wide gap case ($\zeta = 0.3$) and a narrow gap case ($\zeta = 0.9$). The magnetic field strength

Table 4.1. Thermophysical and magnetic properties used in the calculations

Density of the base fluid	ρ_f	997 kg/m^3
Specific heat of the base fluid	c_f	4180 J/kg·K
Thermal conductivity	k	0.58 W/m·K
Viscosity of the base fluid	η_0	9×10^{-4} Pa·s
Thermal coefficient	β	2.57×10^{-4} 1/K
Density of the nanoparticle	ρ_p	5200 kg/m^3
Bulk magnetization of the magnetic particle	M_d	4.5×10^5 A/m
Brownian relaxation time of the magnetic particles	τ_B	10^{-6} s

values are chosen from the interval of $0 \leq H_0[A/m] \leq 10^5$, the temperature difference values are chosen from the interval of $-10 \leq \Delta T[K] \leq 50$, the volume fraction values of magnetic particles (magnetite) are chosen from the interval $0 < \phi < 0.1$ and finally the size of the ferroparticles is varied in the interval of $5 \leq d[nm] \leq 25$. These value ranges correspond to the ranges used in the experiments in the literature. [38]

4.1. Linear Stability

4.1.1. Thermomagnetic effects

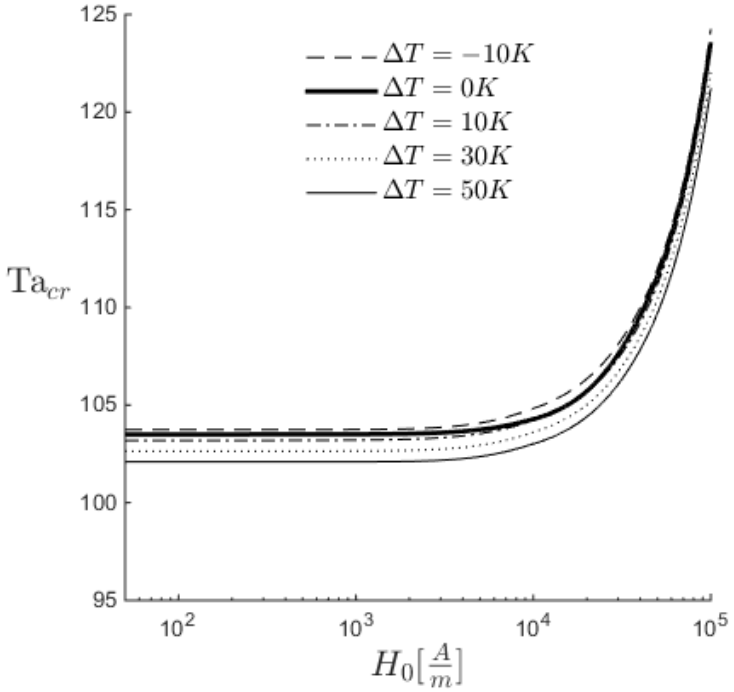

Figure 4.1. Variation of the critical Taylor number with respect to magnetic field strength at different radial temperature differences for $\phi = 0.04$ and $\zeta = 0.3$, the wide-gap case.

The variation of the critical Taylor number with respect to magnetic field strength is shown in Figures 4.1, 4.2 and 4.3 in the wide gap case ($\zeta = 0.3$); in Figures 4.4, 4.5 and 4.6 in the narrow gap case ($\zeta = 0.9$), for different radial temperature differences and ferroparticle volume concentrations, and a particle diameter of $d = 10$ nm. It is seen that strong magnetic fields are required to observe a significant increase in the critical Taylor number, i.e. a significant stabilization for both gap ratios. The magnetic field strength appears in the non-dimensional numbers R_M, κ and also the dimensional parameter c_M which appears in the local Langevin parameter, α_L (defined with Equation (2.14)), and represents the magnetic energy of a single ferroparticle. The magnetic force is scaled with R_M/Re, which corresponds to the ratio of magnetic forces and iner-

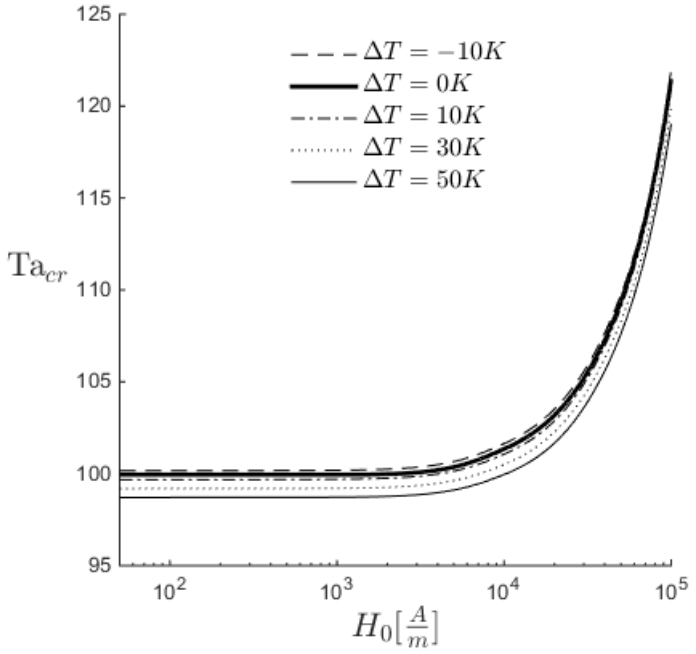

Figure 4.2. Variation of the critical Taylor number with respect to magnetic field strength at different radial temperature differences for $\phi = 0.06$ and $\zeta = 0.3$, the wide-gap case.

tial forces, therefore an increase in R_M would stabilize the flow as it increases the effect of radial Kelvin force over centrifugal force in the momentum equation, Equation (2.2). An upward shift in the local Langevin parameter, α_L, increases the viscosity through the expression (2.15), which also has a stabilizing effect. The parameter κ, which appears in Equation (2.34) and represents the ratio of magnetocaloric energy effects over thermal energy effects as defined in Equation (2.37), is the macroscopic equivalent of the local Langevin parameter, α_L. In the literature, the term $\frac{\partial \mathbf{M}}{\partial T}$ that appears in Equation (2.4) is evaluated using a linear magnetic equation of state and named as pyromagnetic coefficient. [6, 51] However when magnetic relaxation is taken into account, as in this study, $\mathbf{M}$ becomes implicitly dependent on the temperature T therefore the linear magnetic state equation assumption is not suitable. This term appears in Equation (2.4) as a source term that is scaled with κ. It is observed that increasing κ has a destabilizing effect on the flow. The effect of the radial temperature difference can also be seen in Figures 4.1-4.6; an increased temperature non-uniformity leads to flow

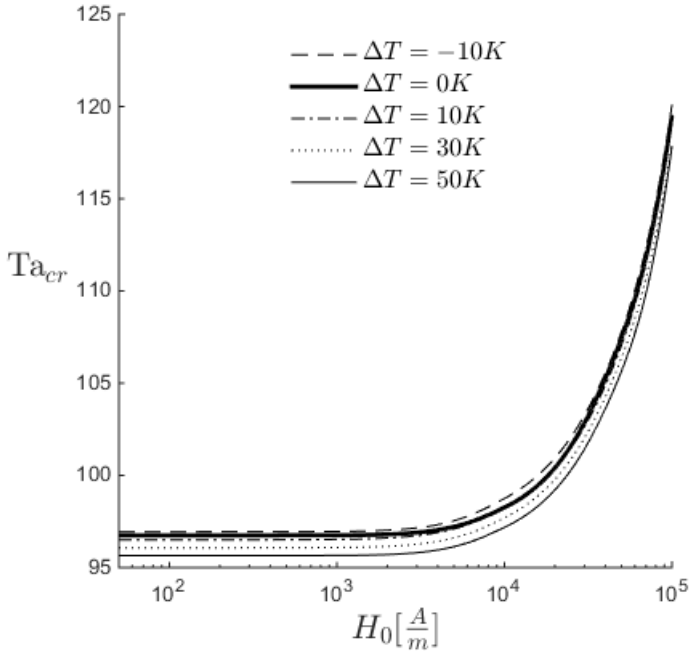

Figure 4.3. Variation of the critical Taylor number with respect to magnetic field strength at different radial temperature differences for $\phi = 0.08$ and $\zeta = 0.3$, the wide-gap case.

destabilization. To illustrate the combined effects of the magnetic field strength and the temperature difference, we plotted a typical case for a concentration of $\phi = 0.06$ in Figure 4.7, for the wide and narrow gap ratios. We can see that destabilizing effect of increasing positive temperature gradient is more pronounced at strong magnetic fields for both gap ratios. Although the temperature effects on the critical Taylor number ratios using these ΔT values seem small, the destabilization trend is clearly detectable. The effect of ΔT appears strongest due to the density change parameter, $c_{\rho,T}$, whose significance on the stabilization is underlined in Sec.3.

The critical wavenumbers, k_{cr}, corresponding to the non-magnetic flow cases have been validated in Sec.3. In the literature, no significant change in the dimensionless critical wavenumber is observed for isothermal flows under azimuthal magnetic fields. [35, 36] For the highest magnetic field strength used in this study ($H_0 = 100$ kA/m), our results indicate a slight decrease of %10 of the critical wavenumber with respect

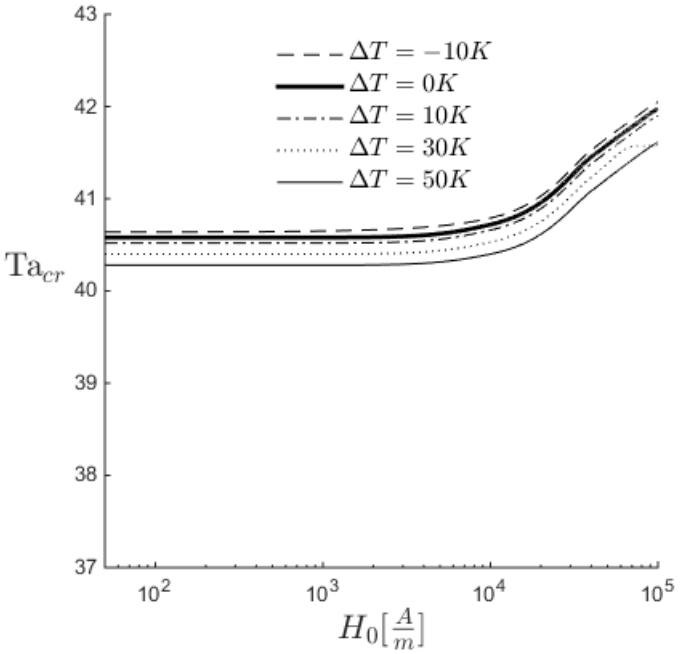

Figure 4.4. Variation of the critical Taylor number with respect to magnetic field strength at different radial temperature differences for $\phi = 0.04$ and $\zeta = 0.9$, the narrow-gap case.

to non-magnetic case where the critical wavenumber $k_{cr} \approx \pi$.

4.1.2. Gap effects

It is well known from the literature that in the absence of magnetic effects, narrowing the gap width has a profound destabilizing effect and decreases the critical Taylor number [25], for both isothermal and non-isothermal flows. This is also validated in Sec.3 (Figure 3.3). It can be observed from Figures 4.4-4.6 that the range of critical Taylor number has decreased to less than 50 percent in the narrow gap case compared to its value in the wide gap case shown in Figures 4.1-4.3. As also shown in Figure 4.7, although the thermomagnetic effects on the stability are similar, these effects are smaller compared to the wide gap case. To illustrate the gap effects more clearly, we plot the critical Taylor number ratio for the isothermal case at a fixed concentration for

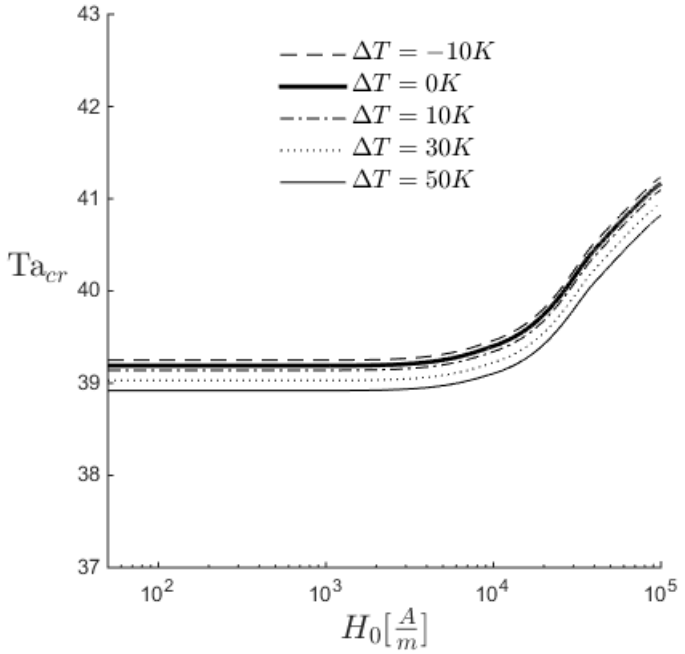

Figure 4.5. Variation of the critical Taylor number with respect to magnetic field strength at different radial temperature differences for $\phi = 0.06$ and $\zeta = 0.9$, the narrow-gap case.

the wide and narrow gap ratios in Figure 4.8. Though the trend of stabilization with increasing magnetic field is similar, the stabilizing effects are weaker in the narrow gap case compared to the wide gap case. This is primarily attributed to the fact that for narrow gap ratios ($\zeta \to 1$), the centrifugal effects become much more dominant than magnetic effects, leading to flow instabilities at much lower Taylor numbers. Also, the wide gap allows a larger change in the magnetic field strength which is essential for the Kelvin force to compete with the centrifugal force. Using the non-dimensional definition of the magnetic field due to an axial line current in Equation (2.16), the range of values for the non-dimensional magnetic field strength is between [1,3.33] in wide gap ($\zeta = 0.3$) whereas in narrow gap ($\zeta = 0.9$) it is between [1,1.11].

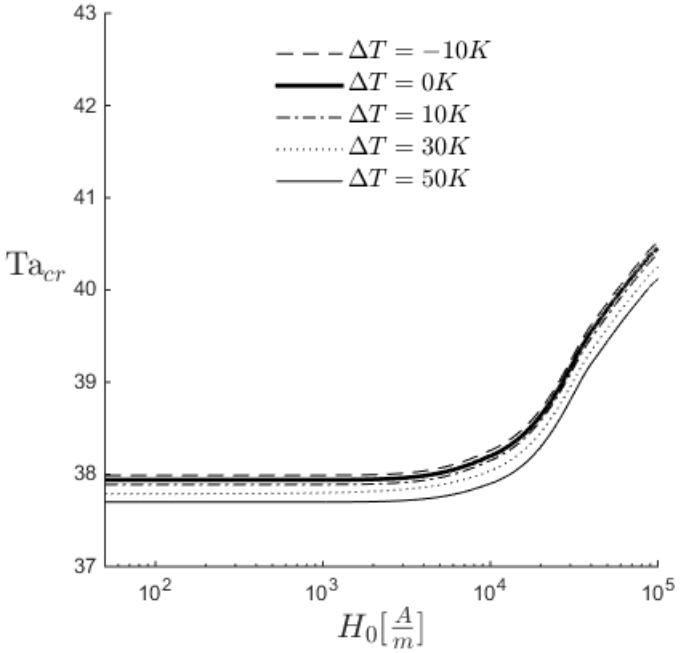

Figure 4.6. Variation of the critical Taylor number with respect to magnetic field strength at different radial temperature differences for $\phi = 0.08$ and $\zeta = 0.9$, the narrow-gap case.

4.1.3. Particle concentration and size effects

The concentration effects are shown in Figure 4.9 for the isothermal case. Higher volume fraction of ferroparticles lead to a stronger stabilization under strong magnetic fields. The volume fraction ϕ is a multiplication factor of the magnetic effects, therefore for the limiting case of $\phi \to 0$ the magnetic effects would vanish, hence higher concentrations magnify the stabilizing effects of the magnetic field strength.

The effect of ferroparticle size is demonstrated for an isothermal flow in Figure 4.10. An increase in the particle size has a considerable effect on the stabilization of the flow under strong magnetic field, especially in the wide gap case, as shown in Figure 4.10. The size of the ferroparticle has an influence on the degree of magnetization of the ferrofluid such that larger particles would result in higher local Langevin parameters and higher degree of magnetization, leading to an increase in both the Kelvin force

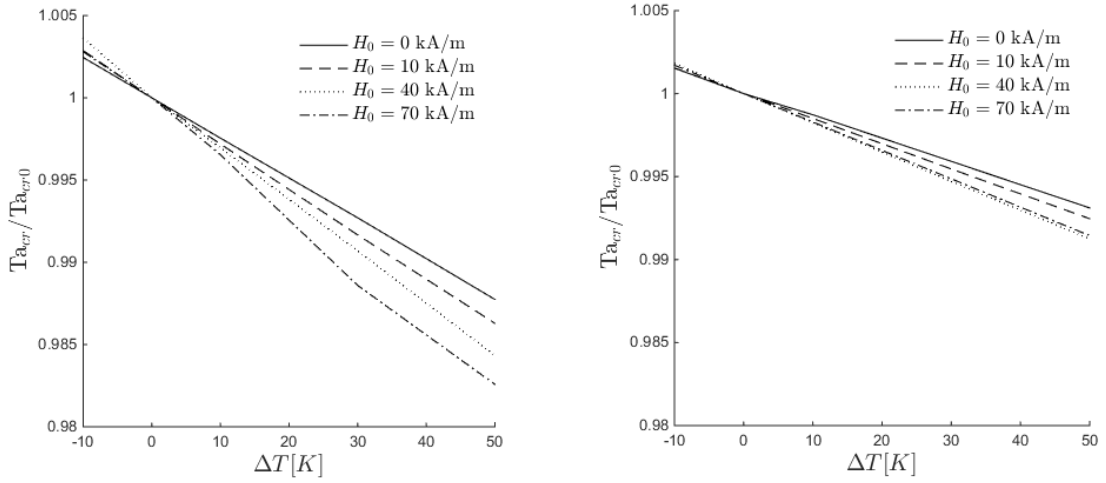

Figure 4.7. Effect of the radial temperature difference on the stability at $\phi = 0.06$. Ta_{cr0} corresponds to the isothermal critical Taylor number at $\phi = 0.06$ for wide gap ($\zeta = 0.3$) (left) for narrow gap ($\zeta = 0.9$) (right)

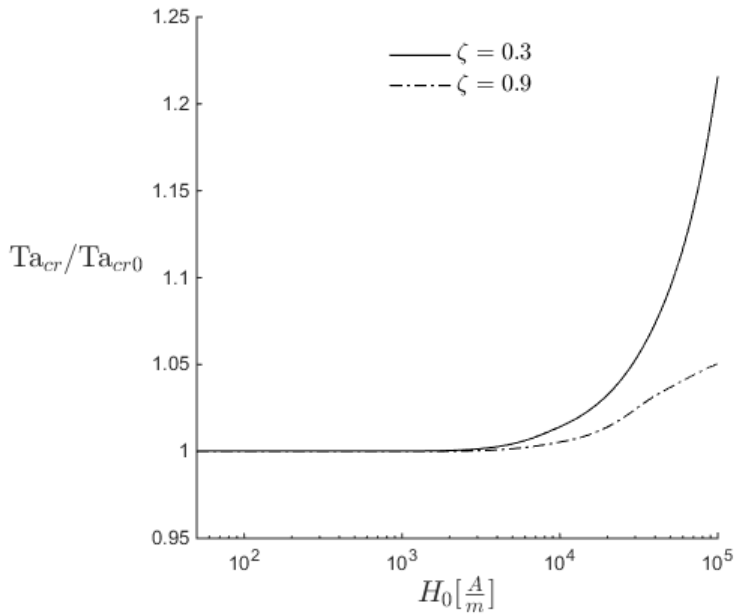

Figure 4.8. Gap effects on the stabilization at $\phi = 0.06$, Ta_{cr0} corresponds to the critical Taylor number for the isothermal case at $\phi = 0.06$ in the absence of the magnetic field.

and the viscosity. One obvious drawback of having a suspension with relatively larger particle size is the magnetic agglomeration and the loss of colloidal stability of the

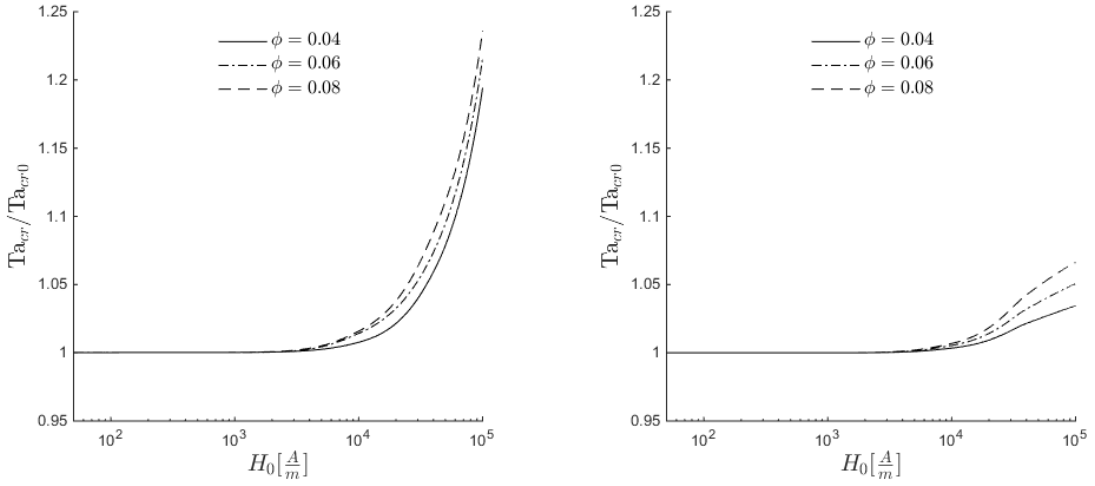

Figure 4.9. Effect of the volume fraction of ferroparticles on the stability. Ta_{cr0} corresponds to the isothermal critical Taylor number in the absence of magnetic field effects for wide gap ($\zeta = 0.3$) (left) for narrow gap ($\zeta = 0.9$) (right)

suspension against gravity. Particle sizes of colloids that are stable to above mentioned mechanisms range up to about 10 nm. [6] We can verify again from Figure 4.10 that for narrow gap ratios, the stabilizing effects are weaker.

4.2. Nonlinear Stability

The nonlinear stability analysis reveal both the eigenfunctions and insight on the onset of the instabilities. The numerical solution of the full system of equations (2.18)-(2.24) given by finite element analysis software COMSOL, show that nonlinear terms have small contribution to the instability mechanisms of the ferrofluid flow in the presence of the magnetic field. The distribution of the radial and axial magnetization field is given for two typical cases at the linear stability boundary. The values shown in Figures 4.11 and 4.12 are normalized with the bulk magnetization of the material which is given in Table 4.1.

Although the instability and the formation of vortical structures are observed at slightly lower Taylor numbers, the results agree with linear stability analysis results

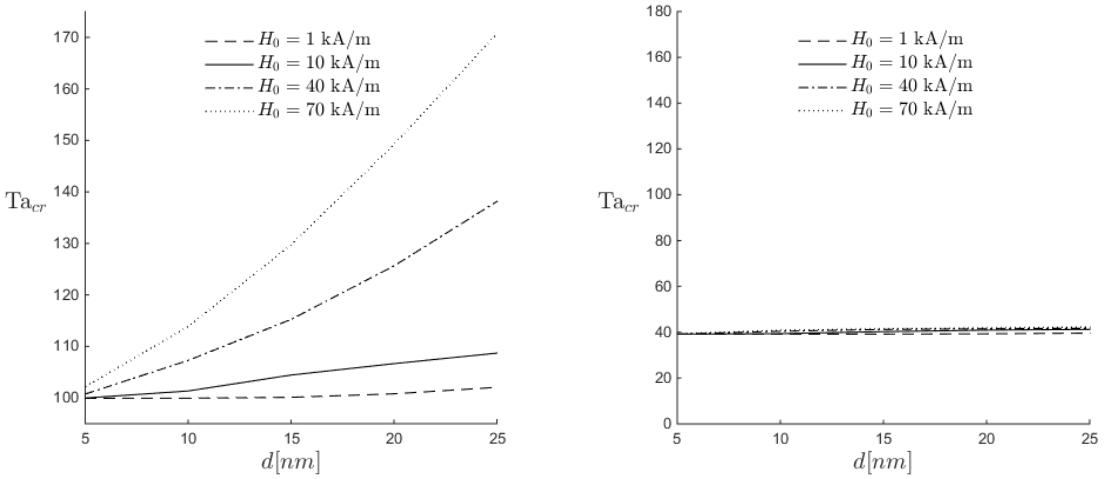

Figure 4.10. The effect of ferroparticle size on the stability at different values of magnetic field strength for wide gap ($\zeta = 0.3$) (left) narrow gap ($\zeta = 0.9$) (right)

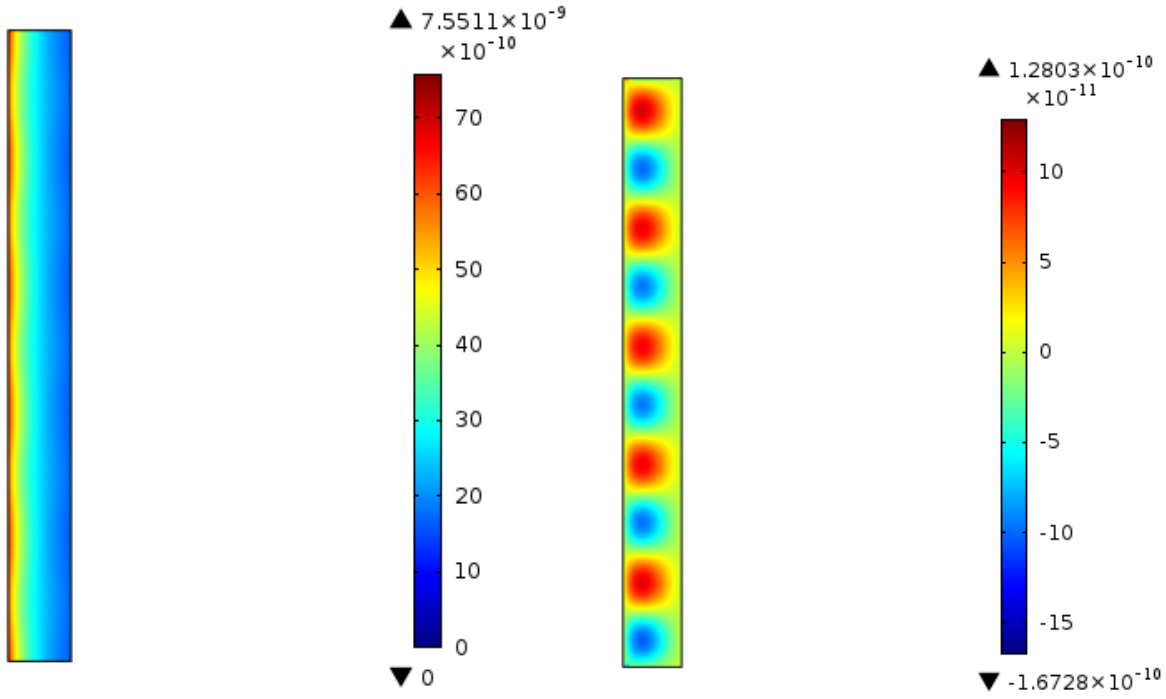

Figure 4.11. In-plane components of the magnetization field $\phi = 0.04$ and $\Delta T = 10$ K, at the corresponding linear Ta_{cr}

showing that the critical Taylor number does not change significantly up to a magnetic field strength of 1 kA/m and having the onset of cellular convection at the Taylor number values given by the linear analysis. Figures 4.11 and 4.12 are obtained at a

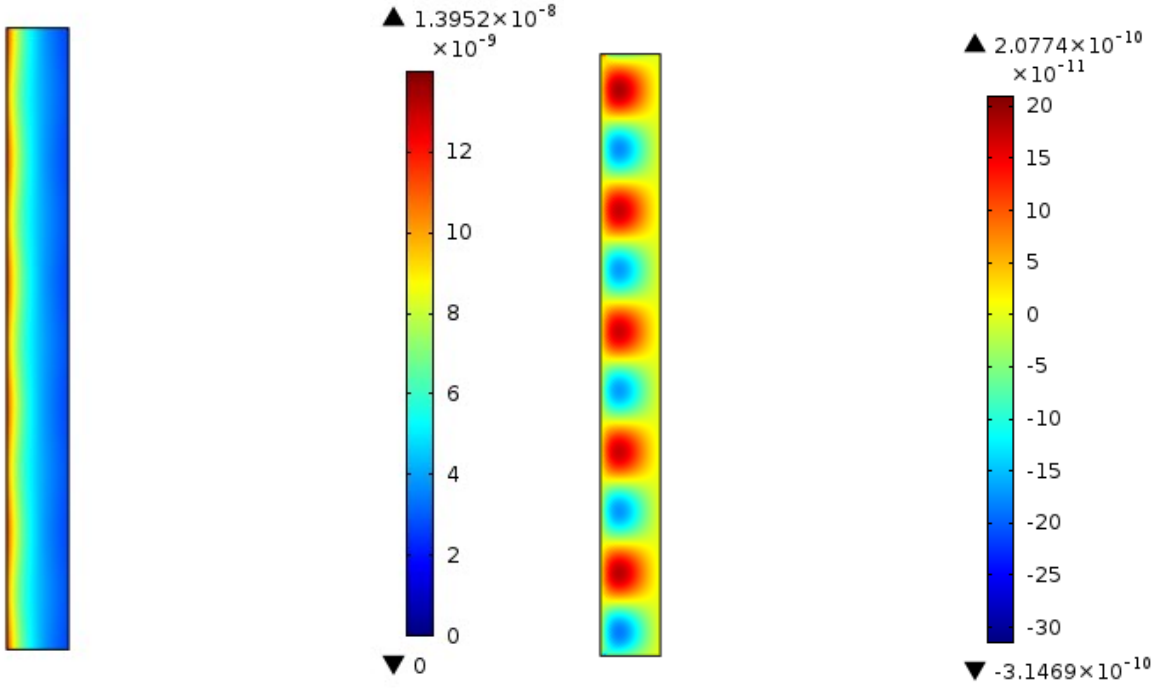

Figure 4.12. In-plane components of the magnetization field $\phi = 0.08$ and $\Delta T = 50$ K, at the corresponding linear Ta_{cr}

magnetic field strength of 1 kA/m.

The corresponding temperature distribution in the annulus is shown in Figure 4.13. It can be seen that the steady state temperature distribution is also perturbed with a wave form even when the governing system of equations are solved directly without linear approximations or introducing normal mode perturbation.

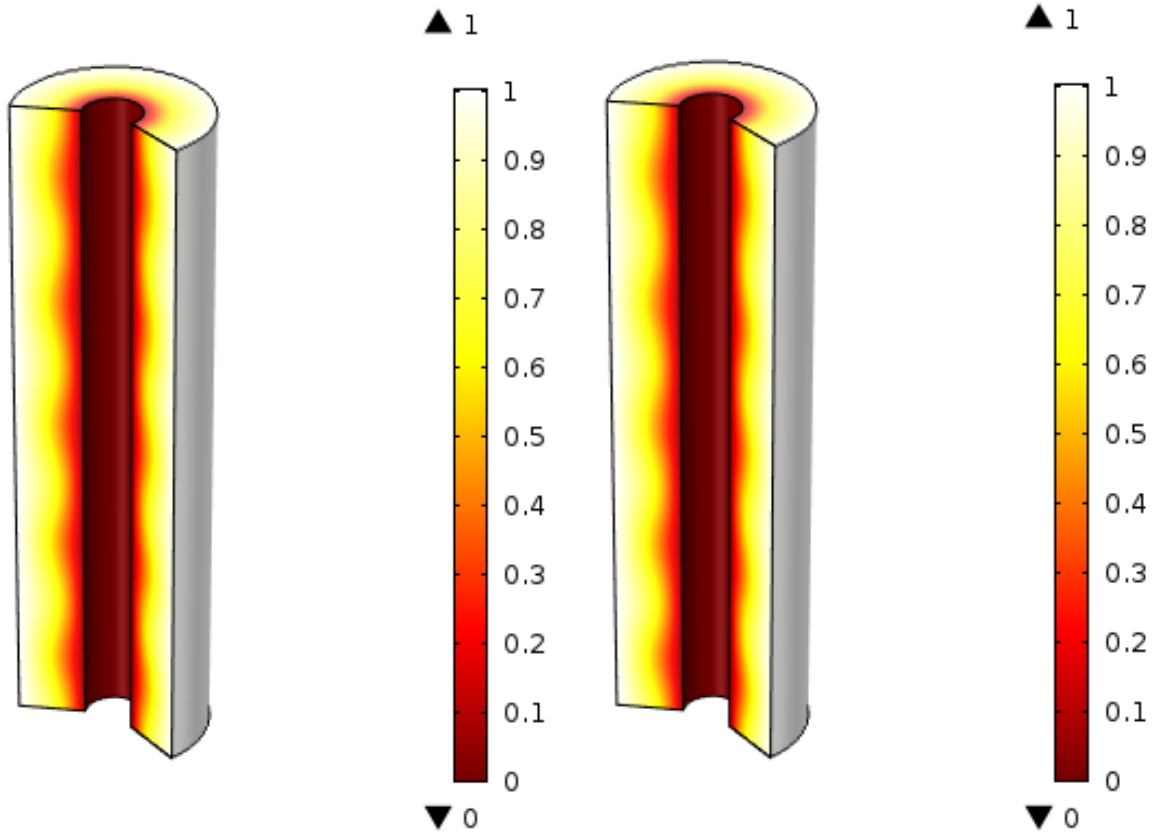

Figure 4.13. The normalized temperature distribution in the annulus at the corresponding linear Ta_{cr} for $\phi = 0.04$, $\Delta T = 10$ K (left) $\phi = 0.08$, $\Delta T = 50$ K (right) at a magnetic field strength of $H_0 = 1\mathrm{kA/m}$

5. CONCLUSION

The thermomagnetic effects on the stability of the Taylor-Couette flow of a ferrofluid in the presence of an azimuthal magnetic field generated by an axial DC current were investigated. A linear stability analysis using Chebyshev collocation method has been applied, also the full nonlinear system of equations has been solved using a finite element software package to reveal the critical Taylor numbers and wavenumbers for the transition from Couette flow to Taylor vortex flow. It is found that significant stabilization may be achieved under the application of strong magnetic fields. Radial temperature difference has a destabilizing effect on the flow and this effect is magnified with increasing magnetic field strength. Ferroparticle volume fraction increases the stabilizing effect of the applied magnetic field by strongly coupling the magnetic effects to the flow. The size of the ferroparticle has also a stabilizing effect which is amplified under stronger magnetic field. These effects are smaller for the narrow gap case where centrifugal effects dominate over magnetic effects.

The work at hand may be extended by including the effects that are neglected in this study such as concentration redistribution and perturbation of the external magnetic field. While magnetoviscous effects are accounted with simple constitutive relations in this work, it is known that nanofluids with tendency to align in longitudinal chains exhibit shear thinning behaviour. Also the magnetic relaxation does lead to viscoelastic behaviour so overall the effects of power law index or elastic effects on the stability of the Taylor-Couette flow should be examined.

Biomedical applications of ferrofluids are also raising in popularity. Taylor-Couette devices are used in red blood cell seperation so a detailed model that accounts for mass diffusion, magnetohydrodynamics and rheology could serve as a benchmark for problems related to blood flow.

REFERENCES

1. Li, Y., S. Tung, E. Schneider, S. Xi, *et al.*, "A review on development of nanofluid preparation and characterization", *Powder Technology*, Vol. 196, No. 2, pp. 89–101, 2009.

2. Akoh, H., Y. Tsukasaki, S. Yatsuya, and A. Tasaki, "Magnetic properties of ferromagnetic ultrafine particles prepared by vacuum evaporation on running oil substrate", *Journal of Crystal Growth*, Vol. 45, pp. 495–500, 1978.

3. Eastman, J. A., S. Choi, S. Li, W. Yu, and L. Thompson, "Anomalously increased effective thermal conductivities of ethylene glycol-based nanofluids containing copper nanoparticles", *Applied physics letters*, Vol. 78, No. 6, pp. 718–720, 2001.

4. Xie, H., J. Wang, T. Xi, Y. Liu, F. Ai, and Q. Wu, "Thermal conductivity enhancement of suspensions containing nanosized alumina particles", *Journal of Applied Physics*, Vol. 91, No. 7, pp. 4568–4572, 2002.

5. Ganguly, R., A. P. Gaind, S. Sen, and I. K. Puri, "Analyzing ferrofluid transport for magnetic drug targeting", *Journal of Magnetism and Magnetic Materials*, Vol. 289, pp. 331–334, 2005.

6. Rosensweig, R. E., *Ferrohydrodynamics*, Courier Corporation, 2013.

7. Afifah, A., S. Syahrullail, and N. Sidik, "Magnetoviscous effect and thermomagnetic convection of magnetic fluid: A review", *Renewable and Sustainable Energy Reviews*, Vol. 55, pp. 1030–1040, 2016.

8. Solis, K. J. and J. E. Martin, "Torque density measurements on vortex fluids produced by symmetry-breaking rational magnetic fields", *Soft Matter*, Vol. 10,

No. 33, pp. 6139–6146, 2014.

9. Cornat, F., D. Beck, I. Jacobi, and H. Stone, "Flow control using ferrofluids", *APS Meeting Abstracts*, 2013.

10. Shapiro, B., "Towards dynamic control of magnetic fields to focus magnetic carriers to targets deep inside the body", *Journal of magnetism and magnetic materials*, Vol. 321, No. 10, pp. 1594–1599, 2009.

11. Nacev, A., C. Beni, O. Bruno, and B. Shapiro, "The behaviors of ferromagnetic nano-particles in and around blood vessels under applied magnetic fields", *Journal of Magnetism and Magnetic Materials*, Vol. 323, No. 6, pp. 651–668, 2011.

12. Li, X., K. Yao, and Z. Liu, "CFD study on the magnetic fluid delivering in the vessel in high-gradient magnetic field", *Journal of Magnetism and Magnetic Materials*, Vol. 320, No. 11, pp. 1753–1758, 2008.

13. Takhar, H. and G. Nath, "Similarity solution of unsteady boundary layer equations with a magnetic field", *Meccanica*, Vol. 32, No. 2, pp. 157–163, 1997.

14. Andersson, H. and O. Valnes, "Flow of a heated ferrofluid over a stretching sheet in the presence of a magnetic dipole", *Acta Mechanica*, Vol. 128, No. 1-2, pp. 39–47, 1998.

15. Ghasemi, S., M. Hatami, A. Salarian, and G. Domairry, "Thermal and fluid analysis on effects of nanofluid outside of a stretching cylinder with magnetic field using Differential Quadrature Method", *Journal of Theoretical and Applied Mechanics*, Vol. 54, No. 2, pp. 517–528, 2016.

16. Dash, G., R. Tripathy, M. Rashidi, and S. Mishra, "Numerical approach to boundary layer stagnation-point flow past a stretching/shrinking sheet", *Journal of*

Molecular Liquids, Vol. 221, pp. 860–866, 2016.

17. Zahn, M., *Electromagnetic Field Theory: a problem solving approach*, John Wiley & Sons, 1979.

18. Ali, M. E., D. Mitra, J. A. Schwille, and R. M. Lueptow, "Hydrodynamic stability of a suspension in cylindrical Couette flow", *Physics of Fluids*, Vol. 14, No. 3, pp. 1236–1243, 2002.

19. Dherbécourt, D., S. Charton, F. Lamadie, S. Cazin, and E. Climent, "Experimental study of enhanced mixing induced by particles in Taylor–Couette flows", *Chemical Engineering Research and Design*, Vol. 108, pp. 109–117, 2016.

20. Akonur, A. and R. M. Lueptow, "Chaotic mixing and transport in wavy Taylor–Couette flow", *Physica D: Nonlinear Phenomena*, Vol. 167, No. 3, pp. 183–196, 2002.

21. Avramenko, A., A. Tyrinov, I. Shevchuk, and N. Dmitrenko, "Centrifugal instability of nanofluids with radial temperature and concentration non-uniformity between co-axial rotating cylinders", *European Journal of Mechanics-B/Fluids*, Vol. 60, pp. 90–98, 2016.

22. Buongiorno, J., "Convective transport in nanofluids", *Journal of Heat Transfer*, Vol. 128, No. 3, pp. 240–250, 2006.

23. Lopez, J. M., F. Marques, and M. Avila, "Conductive and convective heat transfer in fluid flows between differentially heated and rotating cylinders", *International Journal of Heat and Mass Transfer*, Vol. 90, pp. 959–967, 2015.

24. Azaditalab, M., A. Houshmand, and A. Sedaghat, "Numerical study on skin friction reduction of nanofluid flows in a Taylor–Couette system", *Tribology Interna-*

tional, Vol. 94, pp. 329–335, 2016.

25. Taylor, G. I., "Stability of a viscous liquid contained between two rotating cylinders", *Philosophical Transactions of the Royal Society of London. Series A, Containing Papers of a Mathematical or Physical Character*, Vol. 223, pp. 289–343, 1923.

26. Andereck, C. D., S. Liu, and H. L. Swinney, "Flow regimes in a circular Couette system with independently rotating cylinders", *Journal of Fluid Mechanics*, Vol. 164, pp. 155–183, 1986.

27. Fasel, H. and O. Booz, "Numerical investigation of supercritical Taylor-vortex flow for a wide gap", *Journal of Fluid Mechanics*, Vol. 138, pp. 21–52, 1984.

28. Jones, C., "Nonlinear Taylor vortices and their stability", *Journal of Fluid Mechanics*, Vol. 102, pp. 249–261, 1981.

29. Jones, C., "The transition to wavy Taylor vortices", *Journal of Fluid Mechanics*, Vol. 157, pp. 135–162, 1985.

30. Barenghi, C. and C. Jones, "Modulated Taylor–Couette flow", *Journal of Fluid Mechanics*, Vol. 208, pp. 127–160, 1989.

31. Coughlin, K. and P. Marcus, "Modulated waves in Taylor-Couette flow Part 1. analysis", *Journal of Fluid Mechanics*, Vol. 234, pp. 1–18, 1992.

32. Coughlin, K. and P. Marcus, "Modulated waves in Taylor-Couette flow Part 2. numerical simulation", *Journal of Fluid Mechanics*, Vol. 234, pp. 19–46, 1992.

33. Walowit, J., S. Tsao, and R. DiPrima, "Stability of flow between arbitrarily spaced concentric cylindrical surfaces including the effect of a radial temperature gradi-

ent", *Journal of Applied Mechanics*, Vol. 31, No. 4, pp. 585–593, 1964.

34. Ali, M. and P. Weidman, "On the stability of circular Couette flow with radial heating", *Journal of fluid mechanics*, Vol. 220, pp. 53–84, 1990.

35. Niklas, M., "Influence of magnetic fields on Taylor vortex formation in magnetic fluids", *Zeitschrift für Physik B Condensed Matter*, Vol. 68, No. 4, pp. 493–501, 1987.

36. Niklas, M., H. Müller-Krumbhaar, and M. Lücke, "Taylor-vortex flow of ferrofluids in the presence of general magnetic fields", *Journal of magnetism and magnetic materials*, Vol. 81, No. 1-2, pp. 29–38, 1989.

37. Stiles, P. J., M. Kagan, and J. B. Hubbard, "On the Couette-Taylor instability in ferrohydrodynamics", *Journal of colloid and interface science*, Vol. 120, No. 2, pp. 430–438, 1987.

38. Odenbach, S. and H. Gilly, "Taylor vortex flow of magnetic fluids under the influence of an azimuthal magnetic field", *Journal of magnetism and magnetic materials*, Vol. 152, No. 1-2, pp. 123–128, 1996.

39. Stiles, P. and P. Blennerhassett, "Stability of cylindrical Couette flow of a radially magnetized ferrofluid in a radial temperature gradient", *Journal of magnetism and magnetic materials*, Vol. 122, No. 1-3, pp. 207–209, 1993.

40. Shliomis, M. and M. Souhar, "Self-oscillatory convection caused by the Soret effect", *EPL (Europhysics Letters)*, Vol. 49, No. 1, p. 55, 2000.

41. Köhler, W. and S. Wiegand, *Thermal nonequilibrium phenomena in fluid mixtures*, Vol. 584, Springer, 2008.

42. Shliomis, M. I. and B. L. Smorodin, "Convective instability of magnetized ferrofluids", *Journal of Magnetism and Magnetic Materials*, Vol. 252, pp. 197–202, 2002.

43. Shliomis, M. I. and B. L. Smorodin, "Onset of convection in colloids stratified by gravity", *Physical Review E*, Vol. 71, No. 3, p. 036312, 2005.

44. Lopez, J. M., F. Marques, and M. Avila, "The Boussinesq approximation in rapidly rotating flows", *Journal of Fluid Mechanics*, Vol. 737, pp. 56–77, 2013.

45. Papadopoulos, P., P. Vafeas, and P. Hatzikonstantinou, "Ferrofluid pipe flow under the influence of the magnetic field of a cylindrical coil", *Physics of Fluids (1994-present)*, Vol. 24, No. 12, p. 122002, 2012.

46. Hart, J., "Ferromagnetic rotating Couette flow: the role of magnetic viscosity", *Journal of Fluid Mechanics*, Vol. 453, pp. 21–38, 2002.

47. Shliomis, M., "Effective viscosity of magnetic suspensions", *Zh. Eksp. Teor. Fiz*, Vol. 61, No. 2411, p. s1971d, 1971.

48. Fletcher, C. A., *Computational Galerkin Methods*, Springer, 1984.

49. Weideman, J. A. and S. C. Reddy, "A MATLAB differentiation matrix suite", *ACM Transactions on Mathematical Software (TOMS)*, Vol. 26, No. 4, pp. 465–519, 2000.

50. Kundu, P. K. and I. M. Cohen, *Fluid Mechanics*, Elsevier, 2008.

51. Finlayson, B., "Convective instability of ferromagnetic fluids", *Journal of Fluid Mechanics*, Vol. 40, No. 04, pp. 753–767, 1970.

APPENDIX A: RANGES OF THE NONDIMENSIONAL PARAMETERS

The parametric study of linear stability was conducted with dimensional parameters like the magnetic field strength $H_0[A/m]$, the temperature difference between two concentric cylinders, $\Delta T[K]$. Tables A.1 - A.4 show the values of the nondimensional an scaling parameters introduced in Section 2.3 at the parameter ranges studied in this paper.

Table A.1. Values of $c_{\rho,T}$ and c_{MT1} at the parameter range studied in the paper

	$\Delta T[K]$				
	-10	0	10	30	50
$c_{\rho,T}$	-0.00257	0	0.00257	0.00771	0.01285
$c_{MT1}[J]$	$-1.38{\cdot}10^{-22}$	0	$1.38{\cdot}10^{-22}$	$4.14{\cdot}10^{-22}$	$6.90{\cdot}10^{-22}$

Table A.2. Values of R_M at the parameter range studied in the paper

	$H_0[A/m]$							
	0	10^1	10^2	10^3	10^4	$4{\cdot}10^4$	$7{\cdot}10^4$	10^5
R_M	0	$1.11{\cdot}10^5$	$1.11{\cdot}10^6$	$1.11{\cdot}10^7$	$1.11{\cdot}10^8$	$4.45{\cdot}10^8$	$7.78{\cdot}10^8$	$1.11{\cdot}10^8$

Table A.3. Values of $c_M[J]$ at the parameter range studied in this paper

	$H_0[A/m]$							
$d[nm]$	0	10^1	10^2	10^3	10^4	$4{\cdot}10^4$	$7{\cdot}10^4$	10^5
5	0	$3.70{\cdot}10^{-25}$	$3.70{\cdot}10^{-24}$	$3.70{\cdot}10^{-23}$	$3.70{\cdot}10^{-22}$	$1.48{\cdot}10^{-21}$	$2.59{\cdot}10^{-21}$	$3.70{\cdot}10^{-21}$
10	0	$2.96{\cdot}10^{-24}$	$2.96{\cdot}10^{-23}$	$2.96{\cdot}10^{-22}$	$2.96{\cdot}10^{-21}$	$1.18{\cdot}10^{-20}$	$2.07{\cdot}10^{-20}$	$2.96{\cdot}10^{-20}$
15	0	$9.99{\cdot}10^{-24}$	$9.99{\cdot}10^{-23}$	$9.99{\cdot}10^{-22}$	$9.99{\cdot}10^{-21}$	$4.00{\cdot}10^{-20}$	$7.00{\cdot}10^{-20}$	10^{-19}
20	0	$2.37{\cdot}10^{-23}$	$2.37{\cdot}10^{-22}$	$2.37{\cdot}10^{-21}$	$2.37{\cdot}10^{-20}$	$9.47{\cdot}10^{-20}$	$1.66{\cdot}10^{-19}$	$2.37{\cdot}10^{-19}$
25	0	$4.63{\cdot}10^{-23}$	$4.63{\cdot}10^{-22}$	$4.63{\cdot}10^{-21}$	$4.63{\cdot}10^{-20}$	$1.85{\cdot}10^{-19}$	$3.24{\cdot}10^{-19}$	$4.63{\cdot}10^{-19}$

Table A.4. Values of κ at the parameter range studied in this paper

	$H_0[A/m]$							
$\Delta T[K]$	0	10^1	10^2	10^3	10^4	$4{\cdot}10^4$	$7{\cdot}10^4$	10^5
-10	0	$-1.36{\cdot}10^{-7}$	$-1.36{\cdot}10^{-6}$	$-1.36{\cdot}10^{-5}$	$-1.36{\cdot}10^{-4}$	$-5.43{\cdot}10^{-4}$	$-9.50{\cdot}10^{-4}$	$-1.36{\cdot}10^{-4}$
10	0	$1.36{\cdot}10^{-7}$	$1.36{\cdot}10^{-6}$	$1.36{\cdot}10^{-5}$	$1.36{\cdot}10^{-4}$	$5.43{\cdot}10^{-4}$	$9.50{\cdot}10^{-4}$	$1.36{\cdot}10^{-4}$
30	0	$4.52{\cdot}10^{-8}$	$4.52{\cdot}10^{-7}$	$4.52{\cdot}10^{-6}$	$4.52{\cdot}10^{-5}$	$1.81{\cdot}10^{-4}$	$3.17{\cdot}10^{-4}$	$4.52{\cdot}10^{-4}$
50	0	$2.71{\cdot}10^{-8}$	$2.71{\cdot}10^{-7}$	$2.71{\cdot}10^{-6}$	$2.71{\cdot}10^{-5}$	$1.09{\cdot}10^{-4}$	$1.90{\cdot}10^{-4}$	$2.71{\cdot}10^{-4}$

APPENDIX B: TABULATED RESULTS AND EIGENFUNCTIONS

Table B.1. Linear stability results as (k_{cr},Ta_{cr}) pairs for $\phi = 0.04$, $\zeta = 0.3$

	ΔT [K]				
H_0[A/m]	-10	0	10	30	50
0	(3.218, 103.74)	(3.21, 103.48)	(3.206, 103.187)	(3.206, 102.63)	(3.206, 102.1)
10	(3.218, 103.74)	(3.28, 103.493)	(3.206, 103.187)	(3.206, 102.64)	(3.23, 102.1)
100	(3.218, 103.74)	(3.193, 103.5)	(3.218, 103.19)	(3.218, 102.64)	(3.218, 102.1)
1000	(3.218, 103.75)	(3.18, 103.51)	(3.206, 103.21)	(3.206, 102.65)	(3.206, 102.1)
10000	(3.19, 104.824)	(3.21, 104.28)	(3.21, 104.211)	(3.22, 103.607)	(3.21, 103.016)
40000	(3.118, 109.987)	(3.08, 109.6)	(3.105, 109.22)	(3.118, 108.495)	(3.156, 107.836)
70000	(2.99, 116.4)	(2.917, 116.004)	(3.018, 115.522)	(2.97, 114,687)	(2.97, 113.85)
100000	(2.94, 124.254)	(2.917, 123.579)	(2.79, 123.123)	(2.88, 122.08)	(2.82, 121.215)

Table B.2. Linear stability results as (k_{cr},Ta_{cr}) pairs for $\phi = 0.04$, $\zeta = 0.9$

	ΔT [K]				
H_0[A/m]	-10	0	10	30	50
0	(3.118, 40.64)	(3.118, 40.58)	(3.118, 40.52)	(3.118, 40.40)	(3.118, 40.28)
10	(3.105, 40.64)	(3.118, 40.58)	(3.118, 40.52)	(3.118, 40.40)	(3.118, 40.28)
100	(3.105, 40.64)	(3.105, 40.58)	(3.118, 40.52)	(3.118, 40.40)	(3.118, 40.28)
1000	(3.105, 40.65)	(3.143, 40.58)	(3.118, 40.52)	(3.13, 40.40)	(3.118, 40.28)
10000	(3.118, 40.79)	(3.105, 40.72)	(3.118, 40.66)	(3.118, 40.53)	(3.106, 40.4)
40000	(3.105, 41.528)	(3.105, 41.453)	(3.118, 41.378)	(3.105, 41.232)	(3.13, 41.084)
70000	(3.118, 41.857)	(3.13, 41.78)	(3.118, 41.709)	(3.118, 41.564)	(3.13, 41.419)
100000	(3.11, 42.051)	(3.118, 41.977)	(3.12, 41.903)	(3.13, 41.758)	(3.13, 41.614)

Table B.3. Linear stability results as (k_{cr},Ta_{cr}) pairs for $\phi = 0.06$, $\zeta = 0.3$

	ΔT [K]				
H_0[A/m]	-10	0	10	30	50
0	(3.206, 100.17)	(3.218, 99.925)	(3.206, 99.68)	(3.226, 99.196)	(3.206, 98.7)
10	(3.193, 100.17)	(3.28, 99.95)	(3.218, 99.68)	(3.218, 99.19)	(3.218, 98.72)
100	(3.206, 100.17)	(3.18, 99.95)	(3.206, 99.68)	(3.206, 99.1924)	(3.218, 98.712)
1000	(3.206, 100.19)	(3.18, 99.95)	(3.218, 99.7)	(3.218, 99.21)	(3.218, 98.725)
10000	(3.218, 101.641)	(3.206, 101.35)	(3.23, 101.065)	(3.18, 100.505)	(3.19, 99.96)
40000	(3.13, 107.665)	(3.105, 107.274)	(3.13, 106.948)	(3.16, 106.276)	(3.168, 105.593)
70000	(3.068, 114.173)	(2.99, 113.854)	(3.005, 113.46)	(3.005, 112.555)	(3.093, 111.87)
100000	(2.8, 122.015)	(2.84, 121.49)	(2.82, 120.913)	(2.90, 119.979)	(2.94, 119.04)

Table B.4. Linear stability results as (k_{cr},Ta_{cr}) pairs for $\phi = 0.06$, $\zeta = 0.9$

	ΔT [K]				
H_0[A/m]	-10	0	10	30	50
0	(3.118, 39.25)	(3.118, 39.19)	(3.13, 39.14)	(3.118, 39.03)	(3.13, 38.92)
10	(3.105, 39.25)	(3.118, 39.19)	(3.118, 39.14)	(3.118, 39.03)	(3.118, 38.92)
100	(3.105, 39.25)	(3.13, 39.19)	(3.118, 39.14)	(3.118, 39.03)	(3.118, 38.92)
1000	(3.105, 39.25)	(3.143, 39.19)	(3.118, 39.14)	(3.118, 39.03)	(3.13, 38.92)
10000	(3.118, 39.463)	(3.143, 39.402)	(3.118, 39.343)	(3.118, 39.223)	(3.118, 39.105)
40000	(3.118, 40.518)	(3.118, 40.444)	(3.118, 40.373)	(3.13, 40.23)	(3.118, 40.09)
70000	(3.118, 40.98)	(3.118, 40.91)	(3.118, 40.84)	(3.13, 40.7)	(3.13, 40.56)
100000	(3.12, 41.236)	(3.118, 41.166)	(3.11, 41.095)	(3.12, 40.956)	(3.12, 40.819)

Table B.5. Linear stability results as (k_{cr},Ta_{cr}) pairs for $\phi = 0.08$, $\zeta = 0.3$

	ΔT [K]				
H_0[A/m]	-10	0	10	30	50
0	(3.206, 96.944)	(3.193, 96.724)	(3.206, 96.5)	(3.206, 96.07)	(3.206, 95.65)
10	(3.218, 96.94)	(3.243, 96.731)	(3.218, 96.5)	(3.206, 96.07)	(3.218, 95.64)
100	(3.231, 96.94)	(3.155, 96.744)	(3.218, 96.5)	(3.218, 96.07)	(3.206, 95.65)
1000	(3.218, 96.96)	(3.18, 96.755)	(3.193, 96.53)	(3.206, 96.12)	(3.206, 95.68)
10000	(3.18, 98.75)	(3.206, 98.26)	(3.21, 98.223)	(3.19, 97.703)	(3.24, 97.187)
40000	(3.155, 105.553)	(3.093, 105.248)	(3.155, 104.886)	(3.23, 104.258)	(3.168, 103.612)
70000	(2.94, 112.355)	(3.105, 111.861)	(2.93, 111.5)	(2.94, 110.687)	(3.018, 109.881)
100000	(2.88, 120.102)	(2.83, 119.553)	(2.88, 119.02)	(2.97, 117.983)	(2.87, 117.87)

Table B.6. Linear stability results as (k_{cr},Ta_{cr}) pairs for $\phi = 0.08$, $\zeta = 0.9$

	ΔT [K]				
H_0[A/m]	-10	0	10	30	50
0	(3.118, 37.99)	(3.13, 37.94)	(3.118, 37.89)	(3.118, 37.79)	(3.118, 37.7)
10	(3.105, 37.99)	(3.118, 37.93)	(3.118, 37.89)	(3.118, 37.79)	(3.118, 37.7)
100	(3.105, 37.99)	(3.13, 37.93)	(3.118, 37.89)	(3.118, 37.79)	(3.118, 37.7)
1000	(3.118, 37.99)	(3.118, 37.94)	(3.118, 37.89)	(3.13, 37.8)	(3.118, 37.7)
10000	(3.118, 38.26)	(3.143, 38.2)	(3.13, 38.15)	(3.118, 38.04)	(3.118, 37.9)
40000	(3.118, 39.62)	(3.118, 39.55)	(3.118, 39.478)	(3.105, 39.339)	(3.118, 39.2)
70000	(3.118, 40.204)	(3.118, 40.137)	(3.118, 40.069)	(3.118, 39.933)	(3.118, 39.795)
100000	(3.11, 40.519)	(3.118, 40.452)	(3.11, 40.384)	(3.12, 40.251)	(3.12, 40.119)

Table B.7. Linear stability results as (k_{cr},Ta_{cr}) pairs for $\Delta T = 0$ K, $\zeta = 0.3$ and $H_0 = 70$ [kA/m]

	d[nm]				
ϕ	5	10	15	20	25
0.04	(3.23, 105.398)	(2.917, 116.004)	(2.754, 131.89)	(2.45, 151.65)	(2.303, 173.516)
0.06	(3.143, 102.207)	(2.99, 113.854)	(2.817, 129.722)	(2.479, 149.215)	(2.341, 170.703)
0.08	(3.206, 99.189)	(3.105, 111.861)	(2.792, 127.725)	(2.566, 146.966)	(2.291, 168.202)

Table B.8. Linear stability results as (k_{cr},Ta_{cr}) pairs for $\Delta T = 50$ K, $\zeta = 0.3$ and $H_0 = 70$ [kA/m]

	d[nm]				
ϕ	5	10	15	20	25
0.04	(3.143, 103.923)	(2.917, 116.004)	(2.78, 128.903)	(2.56, 147.703)	(2.316, 168.516)
0.06	(3.143, 100.767)	(2.99, 113.854)	(2.78, 126.858)	(2.529, 145.423)	(2.33, 165.922)
0.08	(3.08, 97.906)	(3.105, 111.861)	(2.792, 125.03)	(2.541, 143.397)	(2.303, 163.597)

Table B.9. Linear stability results as (k_{cr},Ta_{cr}) pairs for $\Delta T = 0$ K, $\zeta = 0.9$ and $H_0 = 70$ [kA/m]

	d[nm]				
ϕ	5	10	15	20	25
0.04	(3.118, 40.702)	(3.13, 41.78)	(3.118, 42.257)	(3.13, 42.586)	(3.08, 43.0)
0.06	(3.13, 39.363)	(3.118, 40.91)	(3.118, 41.54)	(3.118, 41.911)	(3.08, 42.328)
0.08	(3.13, 38.155)	(3.118, 40.137)	(3.105, 40.915)	(3.105, 41.322)	(3.09, 41.748)

Table B.10. Linear stability results as (k_{cr},Ta_{cr}) pairs for $\Delta T = 50$ K, $\zeta = 0.9$ and $H_0 = 70$ [kA/m]

	d[nm]				
ϕ	5	10	15	20	25
0.04	(3.13, 40.38)	(3.13, 41.419)	(3.118, 41.9)	(3.118, 42.215)	(3.09, 42.594)
0.06	(3.143, 39.07)	(3.13, 40.56)	(3.13, 41.2)	(3.105, 41.562)	(3.08, 41.953)
0.08	(3.118, 37.886)	(3.118, 39.795)	(3.118, 40.594)	(3.093, 40.995)	(3.105, 41.397)

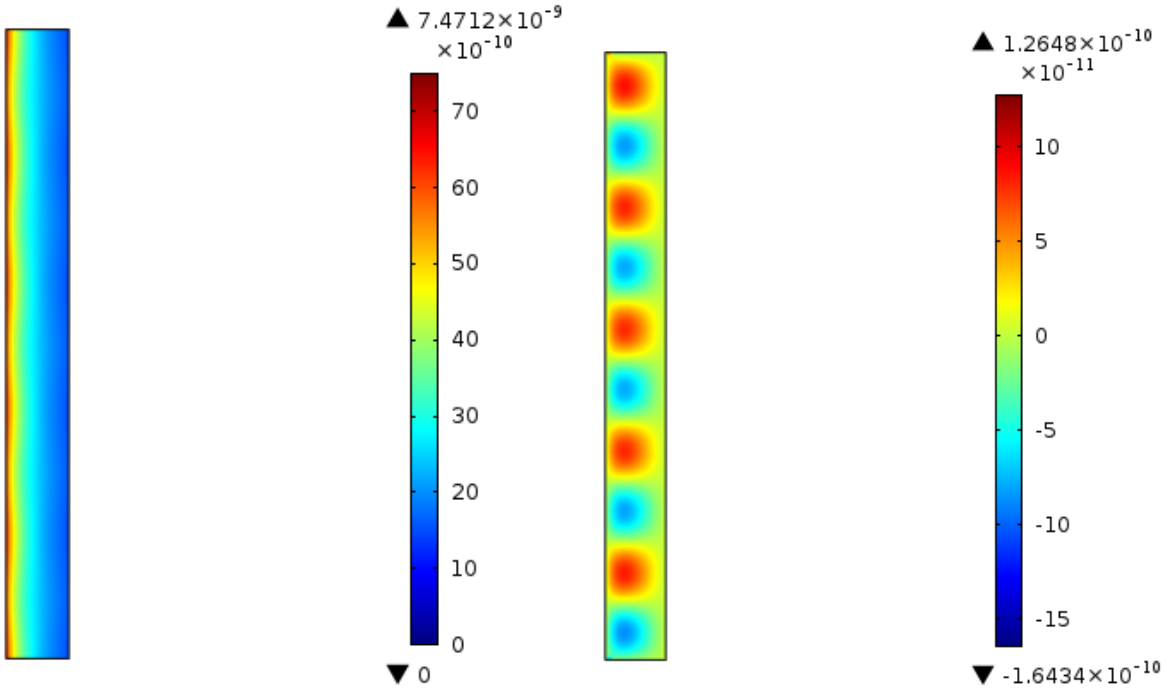

Figure B.1. In-plane components of the magnetization field $\phi = 0.04$ and $\Delta T = 30$ K, at the corresponding linear Ta_{cr}

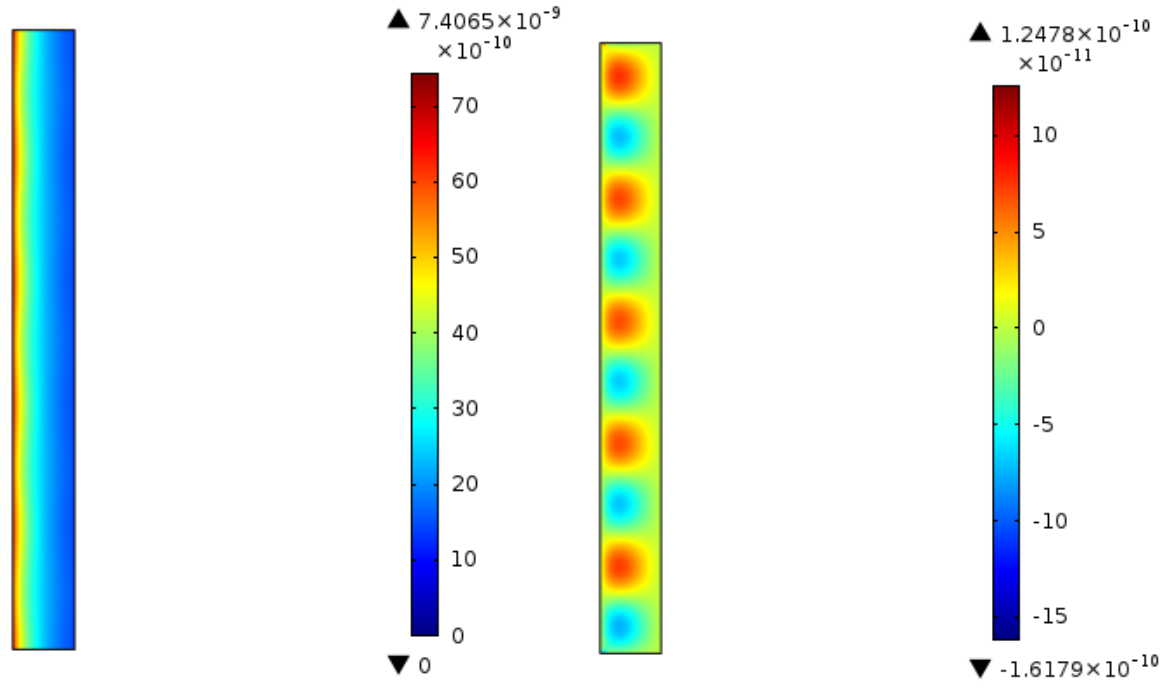

Figure B.2. In-plane components of the magnetization field $\phi = 0.04$ and $\Delta T = 50$ K, at the corresponding linear Ta_{cr}

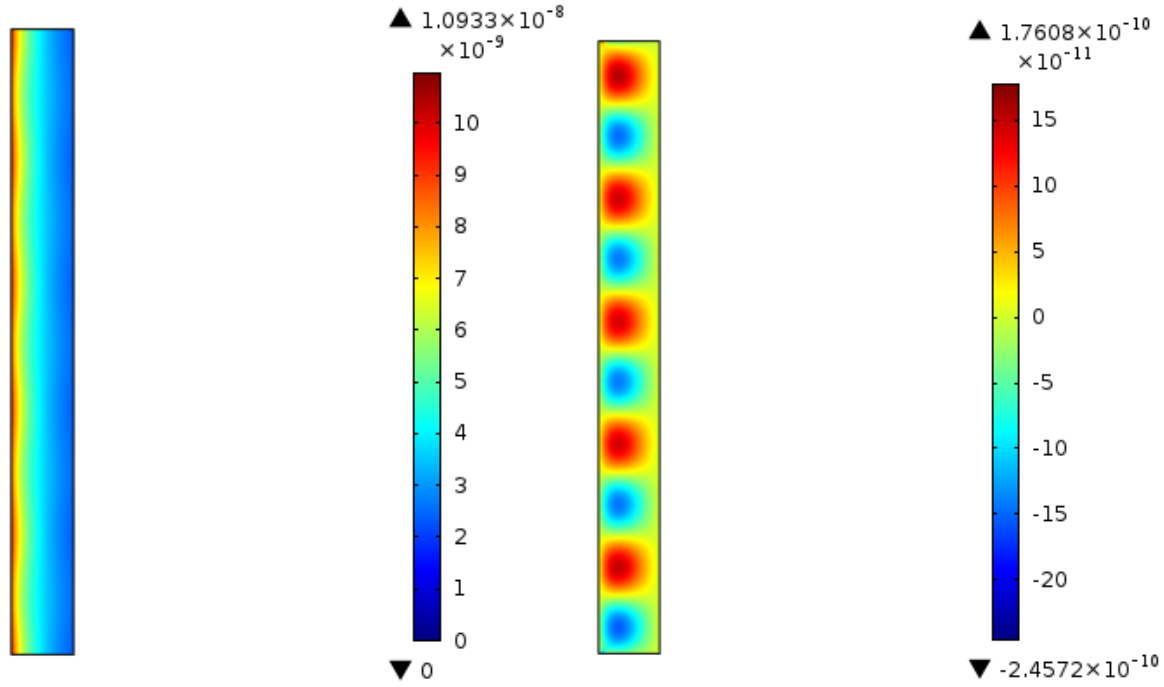

Figure B.3. In-plane components of the magnetization field $\phi = 0.06$ and $\Delta T = 10$ K, at the corresponding linear Ta_{cr}

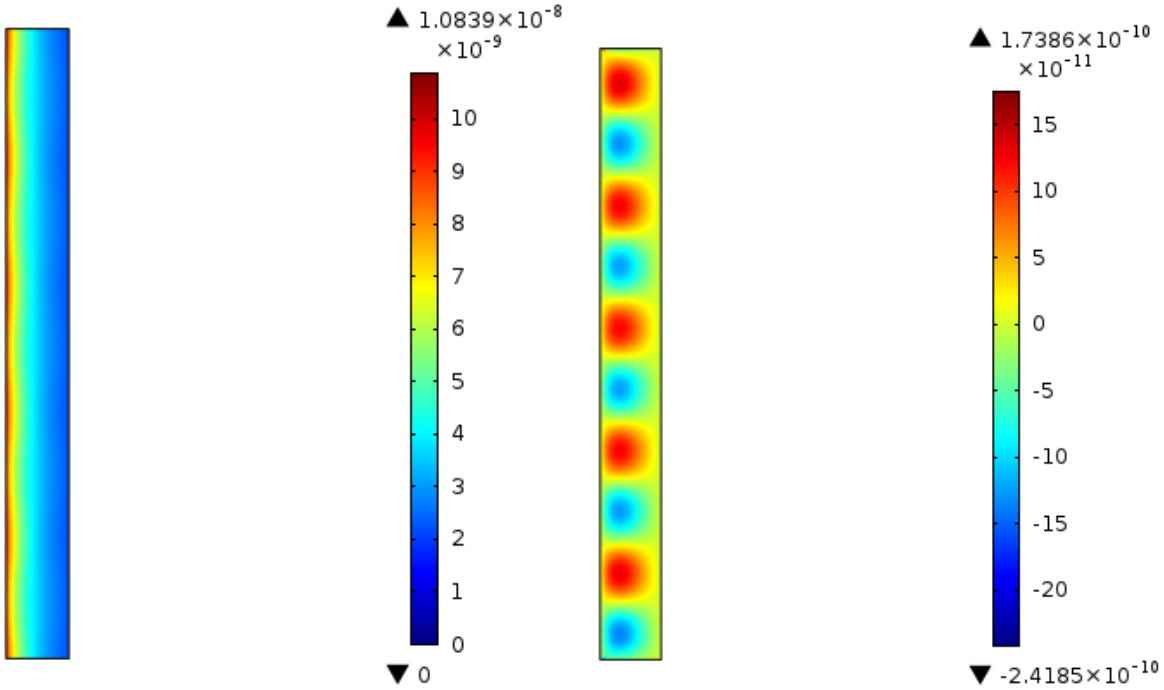

Figure B.4. In-plane components of the magnetization field $\phi = 0.06$ and $\Delta T = 30$ K, at the corresponding linear Ta_{cr}

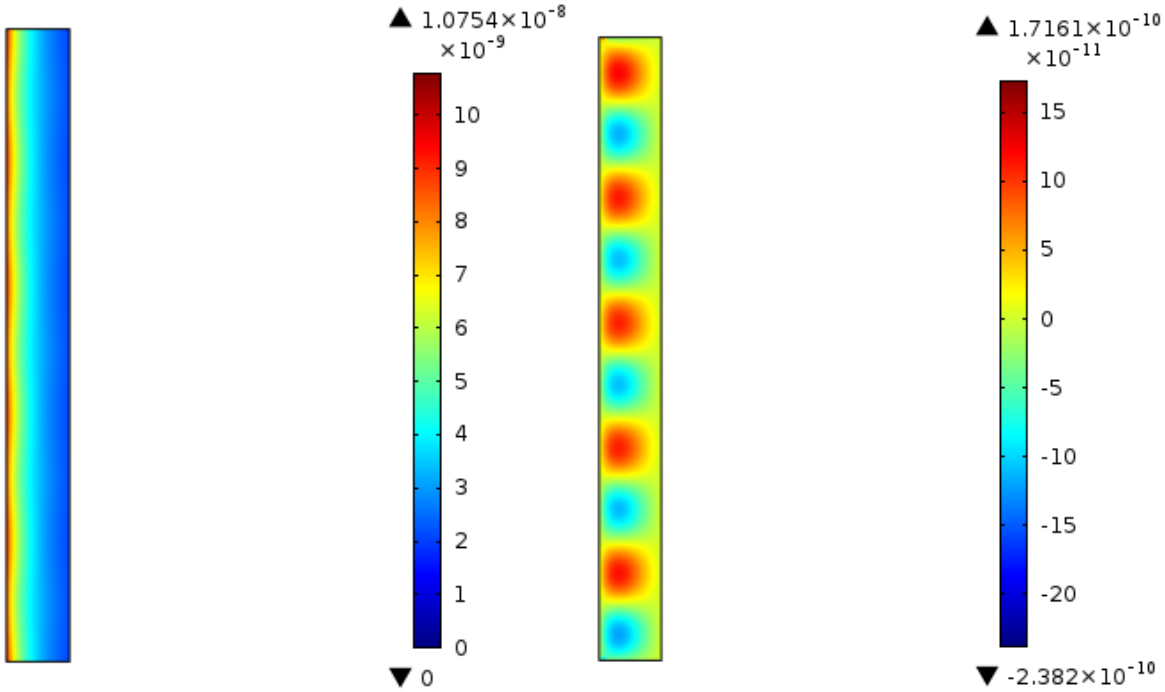

Figure B.5. In-plane components of the magnetization field $\phi = 0.06$ and $\Delta T = 50$ K, at the corresponding linear Ta_{cr}

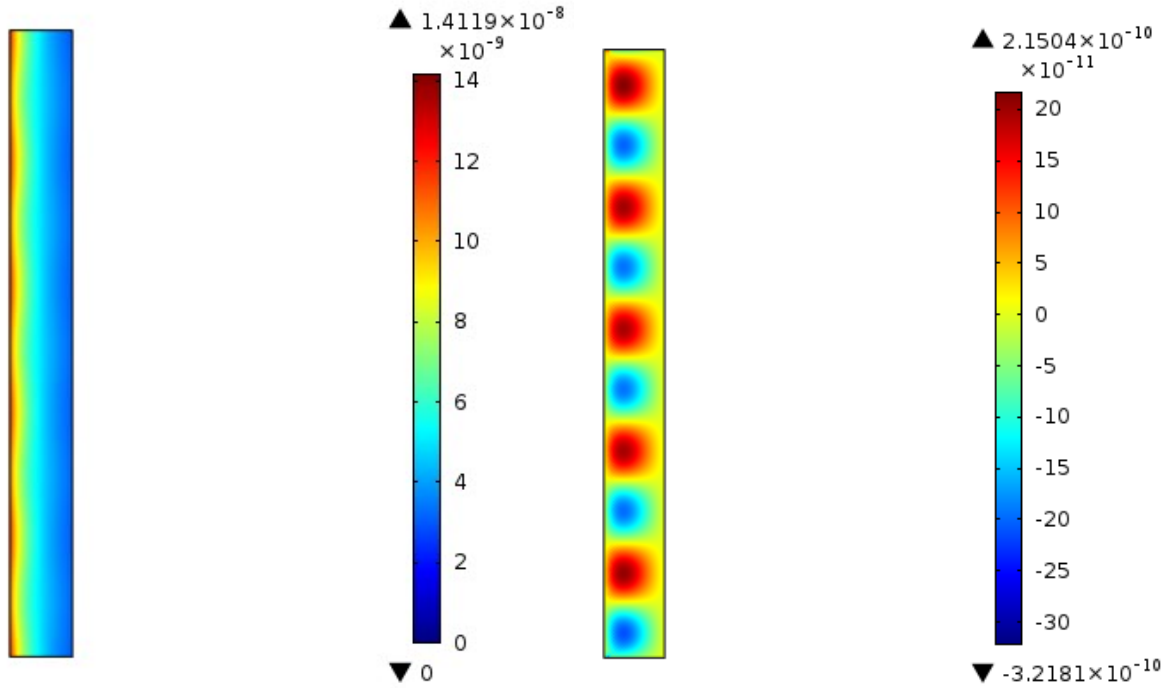

Figure B.6. In-plane components of the magnetization field $\phi = 0.08$ and $\Delta T = 10$ K, at the corresponding linear Ta_{cr}

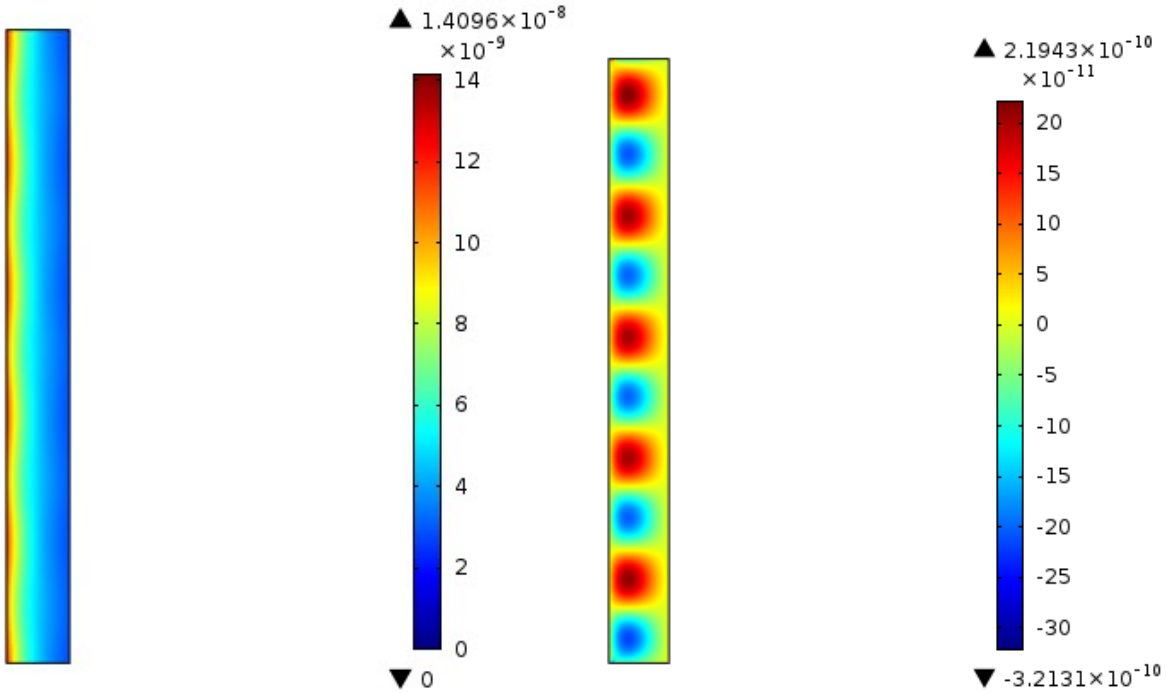

Figure B.7. In-plane components of the magnetization field $\phi = 0.08$ and $\Delta T = 30$ K, at the corresponding linear Ta_{cr}